SAN DIEGO STATE UNIVERSITY AND

UNIVERSITY OF CALIFORNIA

Santa Barbara

Monitoring Forest Cover and Land Use Change in Forest Reserves — Connecting Satellite Imagery to Anthropogenic Impacts

A Dissertation submitted in partial satisfaction of the

requirements for the degree Doctor of Philosophy

in Geography

by

Yu Hsin Tsai

Committee in charge:

Professor Douglas A. Stow, Chair

Professor Li An

Professor Keith C. Clarke

Professor David López-Carr

September 2018

The dissertation of Yu Hsin Tsai is approved.

_____

David López-Carr

_____

Keith C. Clarke

_____

Li An

_____

Douglas A. Stow, Committee Chair

September 2018

Monitoring Forest Cover and Land Use Change in Forest Reserves —

Connecting Satellite Imagery to Anthropogenic Impacts

by

Yu Hsin Tsai

Dedicated To My Beloved Family

VITA OF YU HSIN TSAI
September 2018

EDUCATION

Doctor of Philosophy in Geography, San Diego State University and University of California, Santa Barbara, September 2018 (expected)
Master of Science in Geography, San Diego State University, December 2011
Bachelor of Arts in Geography, National Taiwan Normal University, December 2008

PROFESSIONAL EMPLOYMENT

2013-18: Teaching Associate, Department of Geography, San Diego State University

PUBLICATIONS

Tsai, Y.H., Stow, D.A., Chen, H.L., Lewison, R., An, L., Shi, L., 2018. Mapping vegetation and land use types in Fanjingshan National Nature Reserve using Google Earth Engine. Remote Sens. 10(6), 927.

Coulter, L.L., Stow, D.A., **Tsai**, Y.H., Ibanez, N., Shih, H.C., Kerr, A., Bensa, M., Weeks, J.R., Mensah, F., 2016. Classification and assessment of land cover and land use change in southern Ghana using dense stacks of Landsat 7 ETM+ imagery. Remote Sens. Environ. 184, 396-409.

Stow, D.A., Weeks, J.R., Shih, H.C., Coulter, L.L., Johnson, H., **Tsai**, Y.H., Kerr, A., Benza, M., Mensah, F., 2016. Inter-regional pattern of urbanization in southern Ghana in the first decade of the new millennium. Appl. Geogr. 71, 32-43.

Tsai, Y.H., Stow, D.A., Shi, L., Lewison, R., An, L., 2016. Quantifying canopy fractional cover and change in Fanjingshan National Nature Reserve, China using multi-temporal Landsat imagery. Remote Sens. Lett. 7(7), 671-680.

Stow, D.A., **Tsai**, Y.H., Coulter, L.L., Lippitt, C.D., 2014. Detecting and measuring moving objects with airborne repeat station imaging in rapid succession mode. Remote Sens. Lett. 5(3), 213-220.

Tsai, Y.H., Stow, D.A., Weeks, J.R., 2011. Comparison of object-based image analysis approaches to mapping new buildings in Accra, Ghana using multi-temporal QuickBird satellite imagery. Remote Sens. 3(12), 2707-2726.

FIELDS OF STUDY

Remote sensing, image processing and analysis, spectral mixture analysis, Geographic Information Science, statistical research methods and landscape ecology, survey research methods, vegetation survey, demographic and statistical research

ABSTRACT

Monitoring Forest Cover and Land Use Change in Forest Reserves —
Connecting Satellite Imagery to Anthropogenic Impacts

by

Yu Hsin Tsai

Despite their protected status, forest reserves can be influenced by anthropogenic activities within and adjacent to reserve boundaries, resulting in environmental degradation and changes in forest cover. Long-term monitoring of environmental change within protected areas in a reliable and extensive manner is important given widespread, human-induced land-cover and land-use change. This study demonstrates the utility of optical satellite remotely sensed imagery and multi-temporal image analysis procedures for mapping and monitoring land cover and land use within cloud-prone and mountainous forest reserves and their environs in China and Ghana for the period of mid-1980s to 2018. The novel mapping and monitoring procedures yield extensive land-use dynamic information in a reliable manner by minimizing terrain-related illumination and cloud cover effects. Forest types and land-use are mapped in selected cloud-prone and mountainous forest reserves in China and Ghana to test the reliability of the optimized methods. By applying logical land-use transition rules and interpreting high spatial resolution satellite imagery, land-use changes and the anthropogenic activities associated with them are identified.

Vegetation and land-use types are mapped with moderate to high classification accuracies (64 to 94%) for study areas in China and Ghana. For Fanjingshan National Nature Reserve in China, 12 km^2 in land area is mapped as afforested bamboo and conifer lands associated with payment for ecosystem services programs, and over 25 km^2 is mapped as new development during 1995-2016. Forest area decreased by 9% for the 76 study reserves and environs in southern Ghana between 2000 and 2018. Substantial land changes associated with built development and agricultural expansion are observed in reserve environs within both study areas. Other anthropogenic activities including mining and plantation activities are identified in southern Ghana reserves, while afforestation activities associated with payment for ecosystem programs were predominant adjacent to Fanjingshan in China.

This study contributes to the land-cover and land-use mapping literature by developing and optimizing methods for extremely cloud prevalent and mountainous regions. A semi-automated mapping approach implemented on an open-access, user-friendly platform, similar to the workflow demonstrated in this study, increases the usability and transferability of such mapping techniques. Improved monitoring of other forested, mountainous, and cloud prevalent regions can benefit and inform protected area management and policy, long-term environmental change monitoring, and conservation effort assessment.

TABLE OF CONTENTS

LIST OF FIGURES

LIST OF TABLES

Chapter 1. Introduction

Globally, forests are being depleted at an annual rate of 130,000 km^2 (FAO, 2010)—roughly the size of Greece. Tropical forests in developing countries, such as those in Africa and South America are experiencing forest loss at a higher rate than developed countries. Reports show that the worldwide deforestation rate decreased from over 160,000 km^2 forest loss annually in the 1990s to 130,000 km^2 lost per year in the last decade (FAO, 2010), but estimates of this trend should be treated with caution. Few countries can provide reliable and comparable forest cover change data, thus creating high uncertainty in quantifying the global deforestation rate. In addition, human threats are still prevalent in protected areas (Liu et al., 2001), even when 12% of the world's forest is designated for conservation purposes (FAO, 2010). Forest cover is associated with ecosystem services that are vital to human health and livelihood. As the world becomes more populated, industrialized, and urbanized, more people rely on forest ecosystems for aesthetic value, food, and medicine sources. In order to improve management effectiveness and restore forest resources, mapping and monitoring forest reliably and extensively is key.

Forest reserves are designated forest areas that are protected under the legal systems of many countries. Reserves have different management goals and conservation targets, such as preserving biodiversity and separating threats from the protected areas. To maximize conservation targets, reserves need to be planned systematically, and include distinctive goals and conservation actions to achieve these goals (Margules & Pressey, 2000). Conventional management strategies often involve restricting access of local people to protected areas and traditionally-used resources (Masozera, Alavalapati, Jacobson, & Shrestha, 2006; Hough, 1988), and even displacing people from their lands. These

restrictions can lead to conflicts between reserve management and local people. Potential solutions include gaining trust and communication from the local people, involving residents in decision-making processes, and utilizing community-based management.

To derive information on the spatial distribution and temporal change of surface materials and human usage of the land, vegetation cover and land-use data can be acquired through conventional methods such as field surveys. However, such approaches are not efficient because of time and costs (Cheong, Brown, Kok, & López-Carr, 2012). Remote sensing offers a cost-effective and practical means to map land-cover and land-use, especially over extensive areas. Moderate spatial resolution satellite systems such as Landsat can provide multispectral imagery dating back to the early 1970s, supporting long-term monitoring of forest cover. Much research has focused on mapping vegetation and land-use (Hansen et al., 2013; Xie, Sha, & Yu, 2008), although many of these studies suffered from requiring intense processing requirements, or extensive training data collection prior to mapping. Refined and novel approaches are needed for monitoring forest cover in a simpler way, particularly in developing countries.

This dissertation study builds upon and is part of two funded research projects[1] conducted for portions of China and Ghana, with the focus of this study on land change in and surrounding forest reserves. Historically, both China and Ghana had abundant pristine natural forest resources. During the 1960s and 70s, the majority of forest resources in both countries were consumed by agricultural and urban expansion, and over-exploitation (Harkness, 1998; Appiah et al., 2009). Even though the amount of natural reserves started to

[1] Dynamics of Coupled Natural and Human System program of National Science Foundation (Award DEB-1212183); Interdisciplinary Research in Earth Science program of National Aeronautics and Space Administration (G00009708).

grow in the 80s and 90s, human activities commonly occur in forest reserves and almost all reserves have been selectively logged at some point of time in both countries. In Ghana, logging was so widespread that vegetation outside of reserves is mostly secondary vegetation regeneration on abandoned farms (Hall & Swaine, 1976). As a result of anthropogenic activities, reserves are usually isolated islands of ecosystem in both countries.

In China, human activities within and near forest reserves are common, such as tourism, farming, and reforestation. Financial support for these activities typically comes from state government and local fiscal resources. Tourism is commonly developed in order to generate revenue. Unfortunately, there are few guidelines for sustainable or eco-friendly tourism. Afforestation is another human activity that is relevant to forest resources. China has two of the world's largest payment for ecosystem services (PES) programs, and both aim to increase forest cover and reduce soil erosion. They are often referred to as Grain to Green program (GTGP) and national forest conservation program (NFCP). Both programs originated after a devastating flood causing soil erosion and landslides in 1998, to which deforestation and farming on steep sloped land were major contributors. GTGP encourages afforestation through farmers converting sloped farmland to ecological and timber-producing trees, economic trees, or grassland (Wang et al., 2007). GTGP participants receive crop and cash compensation, free seedlings, and technical support.

In Ghana, rural communities rely especially heavily on forest resources, leading to land degradation and encroachment. Forest related income can take up to 38% of total household income in rural regions (Appiah et al., 2009). Landowners have no incentives to preserve forest resources, especially in off-reserve forests that are owned and managed by individuals or tribal communities. Owubah, Le Master, Bowker, and Lee (2001) estimated that one-third

to two-thirds of the timber harvests come from off-reserve forests in Ghana annually. Reserves in Ghana are designed to yield sustainable production of wildlife, timber and non-timber forest products, and for environment and resource protection. While timber harvesting and mining require permits from the government, they are common activities within reserves. Illegal logging and mining also occur.

The goals of this research are to (1) develop and test novel approaches to map forest cover and monitor its changes, and (2) examine human practices on land-cover and land-use changes in selected forest reserves and their environs in China and Ghana. Reserves in developing countries such as China and Ghana often experience heavy anthropogenic pressure, due to the proximity between growing population and protected areas. Simple and reliable methods are developed to utilize dense time series Landsat imagery for vegetation and land-use change mapping. Furthermore, higher spatial resolution satellite imagery is visually interpreted in conjunction with the Landsat-derived maps to identify possible anthropogenic causes of forest and land-use change. Image processing workflows are implemented on an open-access, web-based geospatial analysis platform to increase the utility of the mapping approach.

The first objective of optimizing methods for monitoring forest cover is described in Chapter 2 and is titled “Mapping vegetation and land-use types in Fanjingshan National Nature Reserve Using Google Earth Engine.” Several image processing techniques, such as multi-seasonal Landsat image composites, ancillary data, spectral vegetation index products, and shade/illumination normalization approaches are explored to map forest and land-use in a reliable manner for a mountainous forest reserve in China. Advanced machine learning image classification routines are implemented to map complex vegetation compositions. The

second objective of examining human practice and land-cover and land-use change in selected reserves in China and Ghana is addressed in Chapters 3 and 4, respectively. Utilizing logical land-use transition rules and building upon the established mapping methods, forest cover and land-use changes are quantified for the reserve in China in Chapter 3—"Monitoring land-cover and land-use dynamics in Fanjingshan National Nature Reserve." The spatial distribution and areal information of new built development and afforestation land are analyzed for the reserve and its environs for a 28-year period. Over 30 years of land-cover and land-use changes are mapped with high accuracy for multiple forest reserves in the extremely cloud prevalent southern Ghana in Chapter 4, which is titled "Monitoring forest cover change with different reserve types in southern Ghana." Dense Landsat image composites and a novel vegetation index are utilized to map forest loss and land-cover transitions. Associated anthropogenic activities are identified for different types of protected area. Lastly, Chapter 5 includes a summary and synthesis of results, important findings, general conclusions, and recommendations for future research.

Chapter 2. Mapping Vegetation and Land-Use Types in Fanjingshan National Nature Reserve Using Google Earth Engine[2]

2.1. Introduction

Despite their protected status, nature reserves can be strongly influenced by adjacent or overlapping anthropogenic activities (Liu et al., 2001). Given this sensitivity, accurately mapping vegetation community and land-use types is important to maintain the integrity of reserve habitat and biodiversity. Fanjingshan National Nature Reserve (FNNR), a national forest reserve in Guizhou province, China, has been identified as one of the 25 global biodiversity hotspots (Myers et al., 2000) with over 100 endemic species. However, human activities such as farming, grazing, tourism, and related development frequently occur from the 21,000 people living within or near the reserve (Wandersee, An, López-Carr, & Yang, 2012).

To protect ecosystem services (limiting soil erosion and runoff) and FNNR biodiversity, Chinese government agencies have implemented payment for ecosystem services (PES) policies to promote afforestation, reduce logging, and limit farming on high sloping lands surrounding the reserve (Uchida, Xu, & Roselle, 2005; Liu et al., 2008; Liu & Yang, 2013). Such PES programs include the National Forest Conservation Program (NFCP) in 1998, seeking to ban logging and promote afforestation to restore forests through incentives paid to forest enterprises or users. One year later, China started another large PES program, the

[2] This chapter was previously published in Remote Sensing: Tsai Y.H., Stow D.A., Chen H.L., Lewison R., An L., Shi L., 2018. Mapping Vegetation and Land Use Types in Fanjingshan National Nature Reserve Using Google Earth Engine. Remote Sens. 10(6), 927. https://doi.org/10.3390/rs10060927

Grain-To-Green Program (GTGP). This program aims to reduce soil erosion and increase vegetation cover through tree planting in steep farmland areas (>15° slope in northwestern China, and 25° in southwestern China; Bennett, 2008; Liu & Diamond, 2005; Chen, Marter-Kenyon, López-Carr, & Liang, 2015). This context makes monitoring and mapping forest vegetation and land-use types an essential element of such programs. At FNNR, these two programs have been implemented for over 16 years, yet quantitative, large scale data about PES effectiveness remains scarce. The reserve management would benefit from mapping and monitoring forest composition and cover in a reliable and extensive manner. While the most feasible and efficient means for such mapping and monitoring is through satellite remote sensing, the persistent cloud cover and steep terrain associated with the FNNR region pose a great challenge to forest mapping with optical or microwave remote sensing approaches.

Landsat satellite imagery has several characteristics that can support long-term mapping and monitoring of vegetation and land-cover changes. Landsat systems provide regular image collection at 30 m spatial resolution with a potential frequency of every 16 days and a freely available image archive dating to the early- to mid-1980s (Xie, Sha, & Yu, 2008). More stable and reliable land change analyses with multi-temporal Landsat data are enabled when digital numbers are converted to surface reflectance values. The conversion to surface reflectance accounts for some atmospheric and solar illumination effects and ensures multi-date images are more comparable (Hall, Strebel, Nickeson, & Goetz, 1991; Moran, Jackson, Slater, & Teillet, 1992). Landsat surface reflectance products are processed through algorithms of the Landsat Ecosystem Disturbance Adaptive Processing System (LEDAPS;

Masek et al., 2006) for Landsat 4, 5 and 7, and Landsat Surface Reflectance Code (LaSRC; Vermote, Justice, Claverie, & Franch, 2016) for Landsat 8 imagery.

Spectral vegetation indices (SVIs) are commonly derived from multispectral images to characterize vegetation. Normalized indices such as simple ratio, normalized difference vegetation index (NDVI), and enhanced vegetation index (EVI) can partially suppress illumination, terrain, and soil reflectance influences in the image data to more reliably monitor vegetation (Qi et al., 1994). For example, EVI was found to be resilient to residual atmospheric effects in a recent study (Davies, Murphy, & Bruce, 2016). Modified soil adjusted vegetation index (MSAVI) and EVI contain a soil adjustment factor that minimizes the soil background while increasing the range of vegetation signal (Qi et al., 1994). MSAVI demonstrated the most linear relationship when regressed with biomass in the Amazonian region among the commonly utilized SVIs (Wang, Qi, & Cochrane, 2005). However, in mountainous regions, the soil adjustment factor was found to cause EVI to be more sensitive to topographic effects when comparing to NDVI (Matsushita et al., 2007). The effectiveness of utilizing various SVIs as input to image classification routines is tested in the mountainous FNNR area in this study.

Compositing or exploiting dense layer stacks of multi-temporal images have been demonstrated to improve forest and land-use type mapping accuracy (Lu & Weng, 2007), though such techniques require managing large quantities of imagery data and exhausting processing resources. Images can be composited to form a multi-layer time series stack to map forest cover, whether they are from the same or different seasons. By compositing multiple images, clouds and other missing data that occur in single images can be ignored, and seasonal phenology signals may be exploited (Franco-Lopez, Ek, & Bauer, 2001).

Potapov, Turubanova, and Hansen (2011) found that Landsat composites of growing season ensured anomaly-free pixels, and was effective in mapping boreal forest cover and change. Forest types were successfully mapped with multi-date Landsat images in New Hampshire (Schriever & Congalton, 1995) and Wisconsin (Wolter, Mladenoff, Host, & Crow, 1995), with accuracies of 74% and 83% respectively. Including ancillary data during the classification has also been found to improve classification accuracy (Xie, Sha, & Yu, 2008; Sluiter & Pebesma, 2010; Domaç & Süzen, 2006). In a steep mountainous study area, Dorren et al. mapped forest types using Landsat Thematic Mapper data and a DEM layer to account for variable illumination effects, with a 73% overall accuracy (Dorren, Maier, & Seijmonsbergen, 2003). A more efficient image processing approach is needed for incorporating different data sources and dense image composites.

Machine learning type classifiers may require larger amounts of training data (Kotsiantis, Zaharakis, & Pintelas, 2007), but higher mapping accuracy can also be achieved than conventional classifiers (Rodriguez-Galiano et al., 2012). A variety of machine learning image classification methods have been used to map vegetation type and land-use, such as artificial neural networks (NN), support vector machine (SVM), decision tree (i.e., CART), and random forest classifiers. SVM classifiers assign pixels to classes by maximizing class separability from the training data, and labels pixels according to their nearest class in feature space (Boser, Guyon, & Vapnik, 1992; Mountrakis, Im, & Ogole, 2011). Decision tree classifiers (Breiman, Friedman, Stone, & Olshen, 1984) apply a multi-stage binary decision making system to classify images. At each stage, pixels are divided according to the binary classification rule. Groups of pixels can be further divided based on tree growing and pruning parameters, until optimal classification is achieved. Decision tree models can be

sensitive to small changes to the training data and parameters (Bishop, 2006). Random forest classifiers construct a multitude of decision trees that are sampled independently during training, typically improving classification results over a single decision tree model (Breiman, 2001; Shelestov et al., 2017). These machine learning classifiers require various input parameters, which can be optimized through cross-validation. In a previous study on classification of natural vegetation in the Mediterranean region, Sluiter and Pebesma (2010) utilized HyMap, ASTER optical bands, and Landsat 7 images and found that machine learning classifiers yielded up to 75% accuracy and outperformed conventional statistical-based classifiers. Johansen, Phinn, and Taylor (2015) mapped woody vegetation in Australia using Landsat 5 and 7 images and concluded that CART and random forest classifiers produced highly accurate vegetation change maps. A study on crop and land-cover mapping in Ukraine compared different machine learning image classifiers, with the highest map accuracy (~75%) achieved with CART (Shelestov et al., 2017). With a random forest classifier and MODIS data, Parente and Ferreira (2018) achieved almost 80% accuracy when mapping pastureland in Brazil. Other studies conclude that random forest classifiers yield higher classification accuracies, require less model training time, and are less sensitive to training sample qualities compared to SVM and NN classifiers (Pal, 2005; Belgiu & Drăguţ, 2016). However, it is not common for remote sensing mapping applications to implement model optimization when utilizing machine learning type image classifiers, a step to ensure better model fitting (Shih, Stow, & Tsai, accepted).

Cloud-computing resources enable efficient image processing on otherwise computational intensive tasks, such as with classification of large volumes of image data, and particularly when using advanced machine learning algorithms. Google Earth Engine

(https://earthengine.google.com/) is a cloud-based platform for geospatial analysis (Gorelick et al., 2017) that is open-access and free of charge for research, education and non-profit purposes. The platform requires a simple online application and a Google user account to access. With a JavaScript code editor platform, Earth Engine provides a massive imagery data collection (including almost the entire Landsat archive and associated surface reflectance products) that can be retrieved directly, allowing users to interactively test and develop algorithms, and preview results in real time. Earth Engine also provides various pixel-based supervised and unsupervised classifiers, including machine learning type algorithms, for mapping implementation. Google Earth Engine was utilized by Hansen et al. (Hansen et al., 2013) to generate global forest cover change products. Over 650 thousand Landsat 7 scenes were incorporated, and the processes took just a few days. Other studies have also demonstrated the ease of incorporating various sources of imagery data and automating image classification routines for crop and vegetation mapping using Earth Engine (Shelestov et al., 2017; Johansen, Phinn, & Taylor, 2015; Parente & Ferreira, 2018).

The objective of this study is to develop and test advanced image classification techniques on the cloud-based platform Google Earth Engine for mapping vegetation and land-use types in the FNNR region and analyze their spatial distributions. A secondary objective is to determine if multi-temporal composites, SVIs, and digital elevation data enable more accurate forest and land-cover mapping results in this cloud-prone and complex terrain study area. Tree-based machine learning image classifiers—decision tree and random forest classifiers are applied to multi-temporal Landsat data to generate vegetation and land-cover maps. Cloud-free multi-seasonal image composites consisting of SVIs and ancillary data are tested for effectiveness in vegetation type mapping. Terrain shading

normalization approaches are implemented to improve the mapping results in the mountainous study area. Vegetation type maps are assessed for accuracy by comparison with reference data collected through field assessment with sampling plots. The vegetation and land-use mapping workflow, which includes cloud-based image processing approaches, provides a reliable method to remotely map forest and land-use composition in FNNR.

2.2. Study Area and Materials

Fanjingshan National Nature Reserve (FNNR, 27.92° N, 108.70° E), as shown in Figure 1, is roughly 419 km^2 in size. FNNR was established in 1978 as a protected area, and included in the UNESCO Man and Biosphere Protection network in 1986. The mountainous terrain displays a vertical elevation difference of over 2000 m and is located in the humid subtropical climate zone. FNNR is also referred to as "ecosystem kingdom", because of its diverse microclimate creates habitat for over 6,000 different types of plants and animals, and over 100 endemic species. The vegetation communities of the FNNR region are complex and normally mixed, and almost no single-species cover type exists (Zhou, 1990). Based on the dominant species, the vegetation communities were generalized into five common types for this study: deciduous, evergreen broadleaf, mixed deciduous and evergreen, bamboo, and conifer. Non-reserve land-use types, namely built and terraced agriculture, tend to be located along the periphery of the forest reserve.

Landsat 5 Thematic Mapper (TM) and Landsat 8 Operational Land imager (OLI) surface reflectance images of FNNR (located within Worldwide Reference System 2 path 126, row 41) on the USGS Earth Explorer website (EarthExplorer, http://earthexplorer.usgs.gov) were reviewed, and selected dates were retrieved from the Google Earth Engine image library for image processing and analysis. Landsat 7 Enhanced Thematic Mapper Plus (ETM+) images

were not utilized for this study due to the Scan Line Corrector failure since 2003. Based on cloud cover and image availability for coverage throughout a vegetation growing season, two study years were selected for this study, 2011 and 2016. Images were also visually

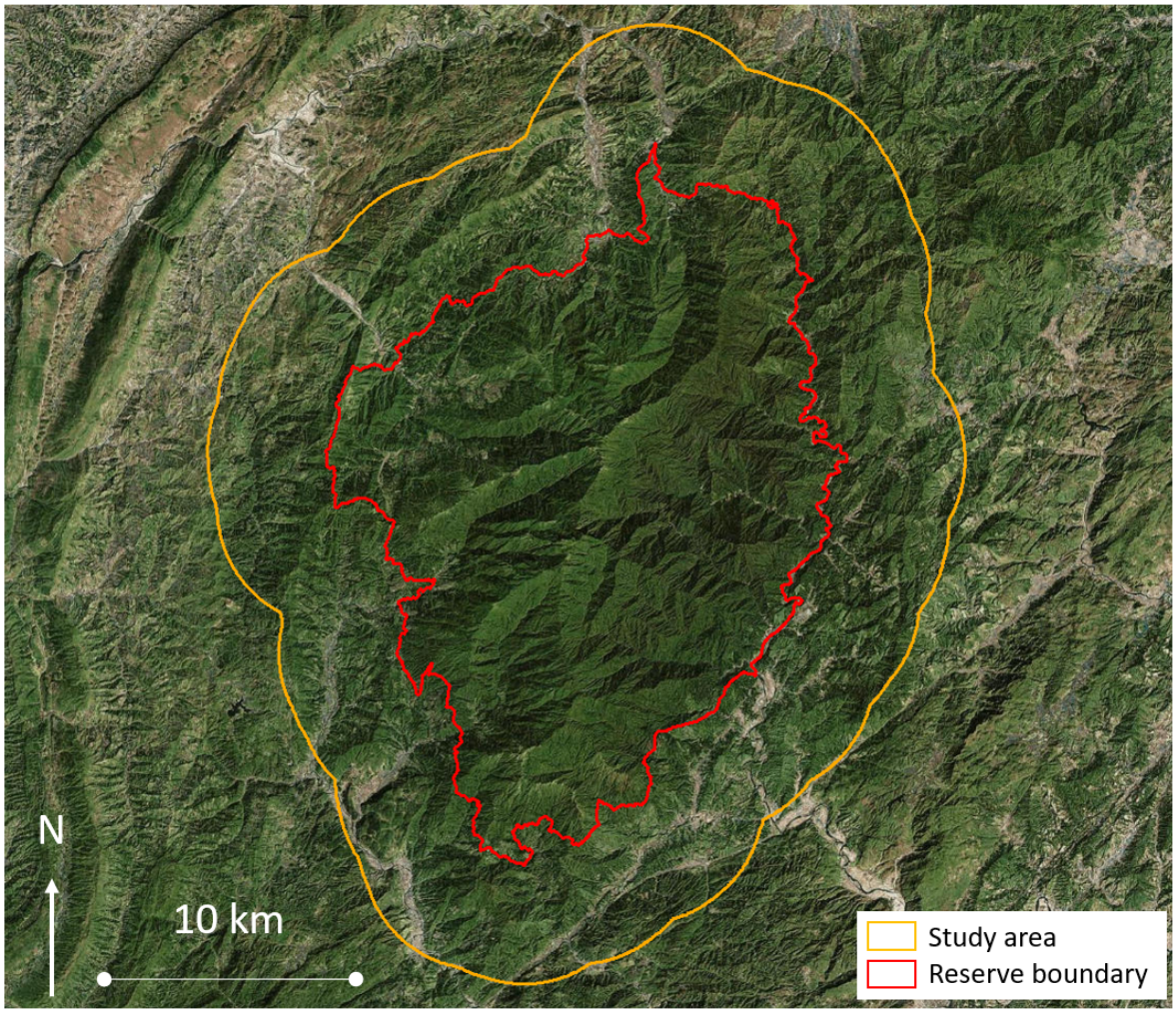

Figure 1. Study area map. Fanjingshan National Nature Reserve boundary is outlined in red; a 6 km buffer based on the reserve boundary shown in orange defines the mapping area for this study. Base imagery source: Esri, DigitalGlobe, GeoEye, Earthstar Geographics, CNES/Airbus DS, USDA, USGS, AeroGRID, IGN, and the GIS User Community.

inspected to ensure the quality of the analysis. Table 1 provides information on specific image dates, sensors, and number of images used.

The FNNR study area is extremely mountainous and cloud-prone. The cloud cover statistics were evaluated with the C version of Function of Mask products (CFmask; Foga et al., 2017) provided with the Landsat LEDAPS/LaSRC processed data sets. Landsat imagery for both study periods contains persistent cloud cover. For the circa 2011 period, portions of the study area have up to ten out of 13 available images that were covered by clouds. A minimum of eight image dates out of 17 images for the circa 2016 period have high amounts of cloud cover. For areas such as the highest ridge and peak located at above 2560 m elevation, there was only one image during the latter study period that provided cloud-free coverage. As Table 1 shows, two mostly cloud-free August images were selected to analyze single-date classification accuracies for 2011 and 2016. Two types of multi-temporal image stacks were also generated for the study periods: cloud-free layerstacks and seasonal composites.

Table 1. Image dates and number of images associated with the study periods for this study.

Study Period & Sensor	**Image Dates**		
	Single Summer Date	**Cloud-Free Layerstack**	**Seasonal Composite**
Circa 2011 Landsat 5	August 16, 2011	November 1, 2010 May 28, 2011 August 16, 2011	2010-2011 13 images
Circa 2016 Landsat 8	August 29, 2016	October 14, 2015 August 29, 2016 May 28, 2017	2015-2016 17 images

Ground reference data on vegetation composition within the portions of the FNNR were collected during Fall 2012, Spring 2013, Spring 2015, Fall 2015, and Spring 2016. Relatively homogeneous 20×20 m^2 and 30×30 m^2 areas were chosen as survey plots, on the ground, based on accessibility and visual inspection. Survey plot locations were selected to ensure sampling within the five common vegetation types in FNNR—deciduous,

evergreen broadleaf, mixed deciduous and evergreen, bamboo, and conifer. At every plot, the dominant vegetation community type was determined based on species cover through a rapid assessment process similar to the California Native Plant Society's Rapid Assessment Protocol (CNPS, 2016). Digital photographs and vegetation structure information was also collected. All the survey plot locations were recorded with a global navigation satellite system receiver.

The survey locations were recorded often under the dense vegetation cover in mountainous terrain in the study area. These factors led to difficulty in collecting more reference data and led to higher degree of uncertainty in positional accuracy. Prior to utilizing the survey data points, the reliability of the reference dataset was improved by cross validating with an unpublished vegetation community map. The vegetation community map was created through a collaborative project between Global Environmental Facility (GEF) and the FNNR management office in 2007. This map was generated through the combination of forest inventory field surveys and visual interpretation of a Landsat image. The map depicted 37 dominant overstory species for the reserve and was rendered to the five common FNNR vegetation community types (i.e., deciduous, evergreen, mixed deciduous and evergreen, bamboo, and conifer). While the map was used as additional reference data, the accuracy of the map has not been determined and differences were observed when comparing the map to high spatial resolution satellite imagery. The locations and vegetation types of the survey data samples were cross-validated and co-located with the GEF 2007 vegetation map. When field assessment and map data did not agree, vegetation type classes were determined using other reference sources, such as PES locations derived from household surveys, high spatial resolution Google Earth images (namely 2013 and 2017

Pleiades), and ArcGIS Basemap imagery (pan-sharpened QuickBird, GeoEye, and WorldView-2 images from 2004 to 2012).

2.3. Methods

The majority of the image processing and analysis for this study was implemented through Google Earth Engine. The methods include image normalization for illumination effects (i.e., shade), generating multi-seasonal image stacks, tuning machine learning classifier parameters, generating classification maps, and assessing accuracies of vegetation/land-use products.

2.3.1. Multi-Temporal Image Stacks

Two types of multi-temporal image stacks were generated: cloud-free layerstacks, and seasonal composites. The cloud-free layerstack image input was formed by stacking the most cloud-free Spring and Fall images available within two consecutive years of the selected Summer image. Images were combined to form a three-date stack. To minimize cloud pixels, seasonal image composites were also generated. For the seasonal composites, all Landsat images that were captured during the years of 2010-2011, and 2015-2016 were utilized. In order for the composites to preserve seasonal vegetation signals, images were split into Spring, Summer, and Fall season groups. For each seasonal group, the mean value between all available images was calculated. Lastly, the three season layers were combined (i.e., layerstacked) to form the seasonal composites.

2.3.2. Classification Feature Input

Due to the extreme elevation range and steep slopes in the FNNR region, a reflectance normalization process was applied to Landsat images by dividing each reflectance band by

the reflectance sum of all bands (Wu, 2004). Spectral band derivatives were utilized to further minimize terrain illumination effects and maximize vegetation signature differences. Six SVIs derived from the reflectance normalized Landsat spectral bands, along with elevation, slope, and aspect layers derived from a SRTM DEM were used as feature inputs for vegetation and land-use classification. The slope layer was calculated in degrees, ranging from 0 to 90°. The aspect layer had a value range from 0 to 360°, and was transformed by taking the trigonometric sine values of aspect to avoid circular data values (Xu et al., 2006). Sine values of aspect represents the degree of east-facing slopes, as the values range from 1 (i.e., east-facing) to -1 (west-facing). Clouds, cloud shadow, and water bodies were masked using the CFmask products.

NDVI, normalized difference blue and red (NDBR), normalized difference green and red (NDGR), normalized difference shortwave infrared and near infrared (NDII), MSAVI, and spectral variability vegetation index (SVVI) were derived from the Landsat data as defined below. MSAVI is calculated as Equation 1 (Qi et al., 1994):

$$\mathrm{MSAVI} = \frac{2\rho_{\mathrm{NIR}} + 1 - \sqrt{(2\rho_{\mathrm{NIR}} + 1)^2 - 8(\rho_{\mathrm{NIR}} - \rho_{\mathrm{red}})}}{2} \quad (1)$$

NDVI is calculated as Equation 2 (Carlson & Ripley, 1997):

$$\mathrm{NDVI} = \frac{\rho_{\mathrm{NIR}} - \rho_{\mathrm{red}}}{\rho_{\mathrm{NIR}} + \rho_{\mathrm{red}}} \quad (2)$$

where ρ_{NIR} and ρ_{red} in Equations 1 and 2 represent the near infrared and red reflectance values for a given pixel. The other three normalized difference indices: NDBR, NDGR, and NDII, were calculated as the form of NDVI in Equation 2, only with blue and red bands for NDBR, green and red bands for NDGR, and infrared bands (NIR and SWIR) for NDII. SVVI is calculated as the difference between standard deviation (SD) of all Landsat bands

(excluding thermal) and SD of all three infrared bands, as displayed in Equation 3 (Coulter et al., 2016):

$$\text{SVVI} = SD(\rho_{\text{all bands}}) - SD(\rho_{\text{NIR and SWIR bands}}) \quad (3)$$

2.3.3. Classifiers

Two pixel-based, supervised machine learning type image classifiers were implemented and tested: decision tree (DT) and random forest (RF). To train and test the image classifiers, forest composition survey data were utilized while agriculture and built sample areas were manually digitized based on high spatial resolution satellite imagery. A total of 109 samples were derived for image classifier training and testing purposes. Of the 109 samples, 34 represented mixed, 12 broadleaf, and eight deciduous vegetation, 16 conifer, 10 bamboo, six bare land, 11 agriculture, and 12 built land uses. These samples were stratified by image illumination to account for the drastic spectral difference between illuminated and shaded slopes (Tsai et al., 2016). The samples were organized in a Google Fusion Table and retrieved in Google Earth Engine. The corresponding input image values for the 109 samples were extracted at the Landsat image pixel level.

Cross-validation and grid search techniques were implemented to optimize classifier parameters and ensure model fitting. The 109 samples were randomly selected and split into two parts (i.e., cross-validation): 2/3 for training and 1/3 for testing. Samples were selected by each class to maintain the class proportion. Different combinations of classifier parameters were systematically tested (i.e., grid search) with the training samples. The trained models were then evaluated using the reserved 1/3 testing samples for the estimated model performance. The parameter combination that yielded the highest testing accuracy was used as the optimal classifier parameter. Final vegetation and land-use maps were

produced based on the optimal classifier parameters utilizing the entire set of data samples. The derived maps portray the five vegetation types (bamboo, conifer, deciduous, evergreen broadleaf, and mixed deciduous and evergreen) and three land-use types: agriculture, bare soil, and built.

2.3.4. Accuracy Assessment

The classification products were evaluated for mapping accuracy using an independent set of accuracy data points. There were difficulties discerning certain forest community types. Thus, the seven-class mapping scheme was generalized into four classes—built, agriculture, forest, and bamboo/conifer vegetation to create a second, more generalized map as part of the accuracy assessment. Conifer and bamboo were grouped into a single class, while the forest class contained deciduous, evergreen, and mixed deciduous and evergreen. A total of 128 points (32 points per class) for the study area were generated using a distance-restricted random method (i.e., points to be at least five Landsat pixels apart) and manual editing. Points were overlaid on the Planet imagery captured on July 2017 (Planet Team, 2018) and manually labeled as forest, bamboo/conifer, agriculture, or built class. The labeled reference points were compared to the corresponding classified pixels, and the percent of agreement was recorded in an accuracy table.

To examine the forest community type classification accuracy, the Landsat-derived classification products for 2011 were compared to the 2007 GEF vegetation map. A spatial correspondence matrix was generated for each product to quantify the site-specific and areal coverage similarities and differences between the classification maps and the GEF map. Only the 2011 classification maps were evaluated for they correspond in time better with the GEF map.

Classification products from the same time period that were derived using different inputs and classifiers were also compared to each other to evaluate differences in classifiers and how they represented the vegetation and land-use of the study area. The most reliable classification approach was determined based on mapping accuracies, and the map comparison and evaluation results between the GEF map and the circa 2011 classification products.

2.4. Results

Figure 2 shows the circa 2016 classification map using RF classifier with the seasonal composite image inputs. The reserve is mostly classified as mixed evergreen and deciduous type (displayed in light green color in Figure 2). Evergreen broadleaf cover (displayed in yellow) has a distinct distribution along the river and stream channels that originate from the reserve, in addition to the concentration on the eastern and southern side of the study area. Deciduous cover type (displayed in brown) is concentrated along the high elevation ridge in the middle of the reserve, as well as the two clusters found on the south end. As for the bamboo and conifer vegetation types, more bamboo cover (displayed in red) is mapped on the eastern side of the reserve, and conifer (displayed in dark green) were found more concentrated to the west and north. The road network that surrounds the reserve is depicted as part of the built class. Mapped in close proximity to built areas are agriculture land, bamboo, and conifer cover types. They are found distributed towards the periphery and outside of the reserve boundary.

Key image classifier parameters were tuned for optimizing the classification accuracies. Optimal parameters were identified for each study period and image input type, and they can be found in Table 2. For the DT classifier, the minimum number of training points required

to create a terminal node was the parameter tuned. Parameters tuned for the RF classifier were number of trees to create, and the number of variables per split.

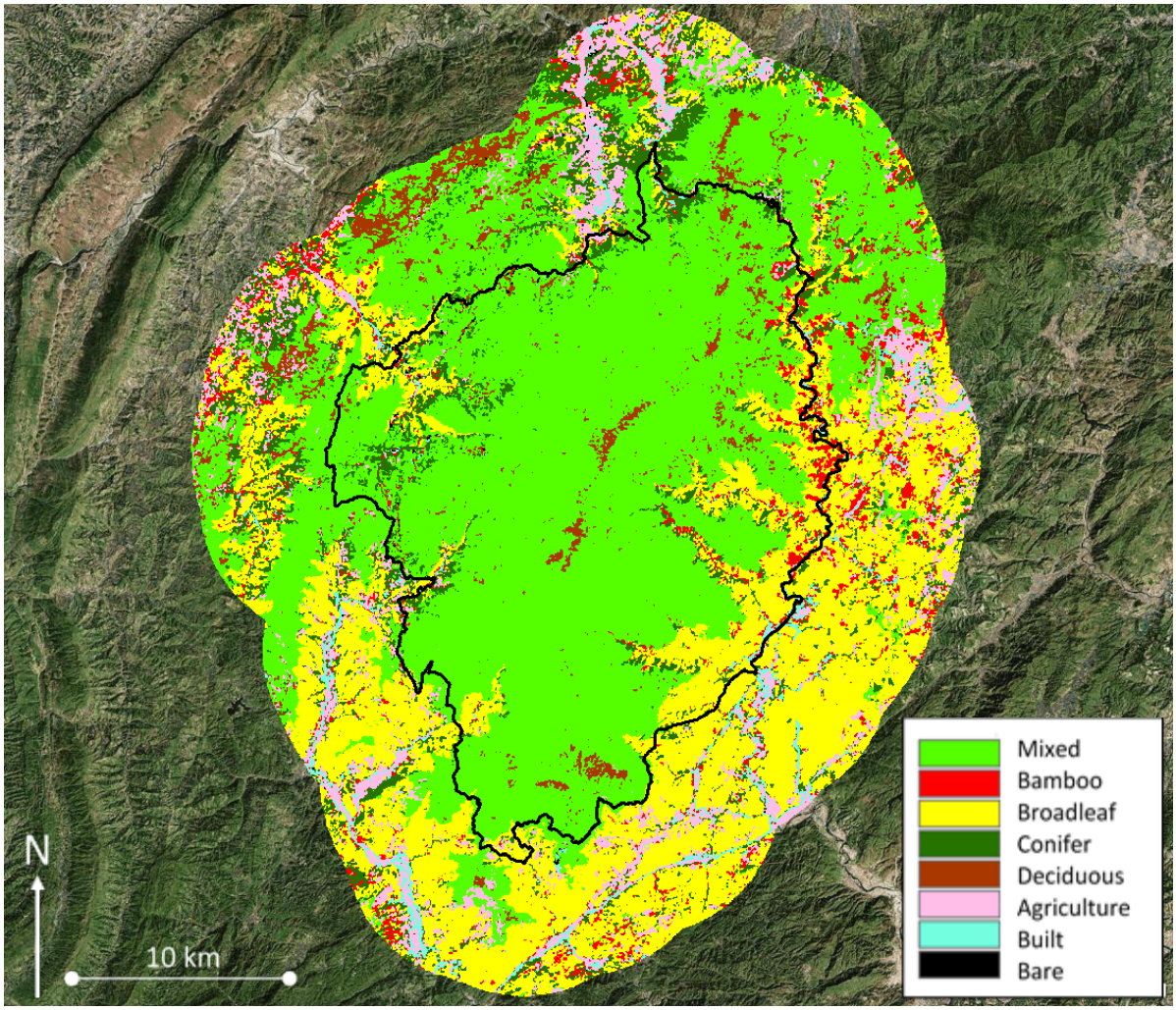

Figure 2. Vegetation type and land-use classification map for circa 2016. The map was derived from the seasonal composite image input with the random forest classifier.

The generalized four-class (i.e., forest, agriculture, built, and bamboo/conifer vegetation) classification map products yielded moderate overall accuracies, particularly with RF classifier with multi-date image inputs. Table 3 shows the generalized map classification accuracies for different study periods and image inputs. Of the classifiers tested, RF classifier consistently yielded higher accuracies compared to the DT classifier (as shown in

Table 3) regardless of study periods or input types. The RF classifier with the circa 2011 cloud-free layerstack image input yielded the highest accuracy value at 77%. Table 3 also shows the multi-image stack approaches yielded higher classification accuracies compared to the single-date input except one instance. On average, the multi-image stack accuracies were 2 to 11% higher. The RF classifier yielded 72 and 74% average accuracies with the multi-image input, while the single date input produced an average accuracy of 65%.

Table 2. The optimal image classifier parameters derived through the grid search tuning. The parameters listed here yielded the highest testing accuracies and were utilized for the final map classifications. Parameters were tuned for decision tree (DT) and random forest (RF) classifiers.

Study Period	**Classifier & Parameters**		**Classification Parameters**		
			Single Summer Date	**Cloud-Free Layerstack**	**Seasonal Composite**
Circa 2011	DT	# of leaf	7	1	2
	RF	# of trees; features	80; 8	133; 2	109; 9
Circa 2016	DT	# of leaf	2	1	1
	RF	# of trees; features	17; 3	11; 5	85; 14

Table 3. The classification accuracy on the generalized, four-class land-cover maps for different study periods and image input types. The average accuracy values are calculated for each input type and image classifier.

Study Period & Classifiers		**Generalized Map Classification Accuracy**		
		Single Summer Date	**Cloud-Free Layerstack**	**Seasonal Composite**
Circa 2011	DT	0.61	0.66	0.67
	RF	0.62	0.77	0.70
Circa 2016	DT	0.64	0.63	0.66
	RF	0.67	0.70	0.73
Average	DT	0.63	0.65	0.67
	RF	0.65	0.74	0.72

Table 4 shows the accuracy assessment results for the circa 2016 period using RF classifier on various methods. Based on classification accuracies and visual inspection,

classification products generated using RF classifier with seasonal composite image inputs yielded the most stable and consistent high accuracy maps. Specifically, the most reliable method (in terms of accuracy and consistency) as seen in Table 4 is utilizing SVIs derived from shade and illumination normalized data in conjunction with a DEM layer as the classification input. This most reliable method yielded 73% mapping accuracy, and is significantly higher compared to using spectral bands (accuracy = 55%). Incorporating elevation information from SRTM DEM as part of the classification input also substantially improved the classification accuracy. RF classification without the DEM layer yielded 66% accuracy, seven percent lower compared to the optimal method. Classification accuracy was slightly lower when using image inputs normalized for shade and illumination, compared to using the non-normalized input products (the excluding normalization method in Table 4). However, without the normalization procedure, the classification result portrayed a substantial amount of conifer misclassification due to the extreme terrain shading in the study area.

Table 5 shows the accuracy assessment and confusion matrix for the circa 2016 classification product that was generated with RF classifier using the seasonal composite image input. The forest class is likely overclassified, suggested by 97% producer's accuracy with a lower, 58% user's accuracy as Table 5 shows. Agriculture land and bamboo/conifer vegetation were the sources of confusion with the forest class. On the other hand, the built class yielded 100% user's accuracy with a lower producer's accuracy (69%), which indicate under-classification. Most of the confusion for the built class is with agriculture land, as small villages and fallow or emergent croplands exhibit similar image signatures. Agriculture activities in the study area are mostly sparse and low stature plantations, which

exposes a lot of bare soil. The high reflectance spectral signature of exposed soil and fallow fields could be the source of misclassification between agriculture and built.

Table 4. Mapping accuracies for circa 2016 using random forest classifier on various seasonal composite image inputs. The x symbols mark the techniques applied, and the mapping accuracy is listed for each method.

Method	**Technique**				**Map Accuracy**
	SVIs	**SRTM DEM**	**Shade Stratification**	**Illumination Normalization**	
Most Reliable Method	x	x	x	x	73%
Spectral Input		x	x	x	55%
Excluding DEM	x		x	x	66%
Excluding Normalization	x	x			79%

Table 5. Accuracy assessment results for the c. 2016 classification product generated with the seasonal composite image input and random forest classifier. These values were derived using the final accuracy assessment data on the four-class generalized map. Gray cells indicate agreement.

c. 2016 Classified Class	**2016 Reference Class**				**User's Accuracy**
	Forest	Agriculture	Built	Bamboo/ Conifer	
Forest	31	9	2	11	58%
Agriculture	0	19	8	0	70%
Built	0	0	22	0	100%
Bamboo/Conifer	1	4	0	21	81%
Producer's Accuracy	97%	59%	69%	66%	Overall Accuracy 73%

The spatial correspondence products generated comparing the circa 2011 classification map (generated using RF classifier with the seasonal composite image inputs) to the GEF reference map indicated 53% of the reserve area was classified as the same vegetation community types as the reference map. Mixed deciduous and evergreen, evergreen

broadleaf, and conifer types were the three classes that showed highest mapping agreement. Most of the reserve core and eastern side of the reserve indicated high agreement, mostly consisting of mixed deciduous and evergreen, evergreen broadleaf, and bamboo types. The north-western portion of FNNR also showed high mapping agreement, and consisting mostly of conifer cover. The Landsat classification maps portrayed the south-western side of the reserve mostly as mixed deciduous and evergreen community types, which made up 30% of the reserve. The same area on the reference map is identified as more heterogeneous, distinguished communities of dominant evergreen broadleaf, deciduous, and conifer. Two ridges to the south of the reserve are mapped as deciduous type cover surrounded by mixed vegetation. The deciduous community makes up roughly 2% of the reserve area. This area is correctly mapped with the Landsat-derived classification products, while the GEF map portrays it as mixed deciduous and evergreen type.

2.5. Discussion

The cloud-based, multi-temporal composite classification approach of satellite-based land-cover data described in this study overcame challenges associated with persistent cloud cover and terrain shading effects in the FNNR region. The results suggest Google Earth Engine is efficient and effective in accessing pre-processed satellite imagery, implementing machine learning type image classifiers, and generating classification products for FNNR. The entire workflow described in this study on average takes less than 30 minutes to complete. The open-access platform and the procedures described in this study enable reserve managers to monitor protected areas in an effective manner without having to purchase or download data and software. The scripting also allows users to streamline complex image processing workflow, and execute processes with minimum intervention.

Collaborating and sharing scripts is also efficient with the online platform. Like most commercial image processing software, Google Earth Engine provides online documentation and tutorials as user support. It also has a discussion forum where users can post questions and share their knowledge. Earth Engine requires no specific hardware setup like most commercial image processing software. However, it does require stable internet connection which might not always be available.

Based on the classification accuracies and visual inspection, classification products generated with RF classifier using seasonal composite image input yielded the most stable, consistent, and accurate maps for the study area. The accuracy assessment results were comparable with many studies mapping mixed forest types in mountainous terrain (Schriever & Congalton, 1995; Sluiter & Pebesma, 2010; Dorren, Maier, & Seijmonsbergen, 2003). Higher mapping accuracy would likely be achieved with larger and more certain training datasets (Kotsiantis, Zaharakis, & Pintelas, 2007; Johansen, Phinn, & Taylor, 2015). Shade and illumination normalization techniques were helpful in minimizing the terrain shading effects and greatly decreased the misclassification of conifer cover. Incorporating elevation and its derived products in addition to SVI layers were also found to improve the classification accuracy and mapping quality significantly. The scaled sine values of the aspect data, which measures east-ness, was found to increase the map accuracy. Likely due to most of the mountain ridges in FNNR being north-south oriented and slopes are facing east-west, the scaled aspect layer using sine function produced higher accuracy than aspect layer scaled by cosine values (which measures north-ness).

The cloud cover issue for FNNR is effectively minimized with the multi-temporal seasonal composite approach, and the RF image classifiers. Cloud cover is prevalent in most

of the Landsat images utilized in this study. The CFmask products were used to exclude cloud pixels prior to image classification, and the pixels were treated as no data values. Utilizing all available data within each season maximizes the amount of cloud-free observations, thus reducing misclassification of no data pixels. Both the single summer date and cloud-free layerstack classification approaches yielded map products with apparent and substantial misclassification due to no data pixels originated from cloud cover. The DT classifier also produced map products with mislabeled no data pixels. In those instances, pixels were commonly mislabeled as bare, agriculture, or built classes. The RF image classifier tested in this study were able to consistently minimize the effects of clouds and the derived no data pixels.

The Landsat-based vegetation type classifications for the core and eastern portion of the FNNR reserve were generally similar to those portrayed in the GEF reference map. The majority of the disagreement occurred at the forest community type level, particularly mixed deciduous and evergreen class. With relatively heavy anthropogenic activities in the western portion of the reserve, it was documented that the pristine, primary forest cover has degraded to mixed primary and secondary forest type, particularly in the lower elevations (Zhou, 1990). This could explain the mapping differences between the classification products and the GEF reference map. A combination of subjective survey work and limited training samples are also likely why the mixed type was not further discerned into evergreen broadleaf or deciduous as in the GEF map. The GEF mapping incorporated forest inventory survey knowledge and was susceptible to labeling biases. The field survey efforts were constrained by the steep terrain and access restrictions from the Reserve Administration Office. There were only a dozen training samples collected in this portion of the reserve,

nine of which were labeled as mixed through fieldwork, and only two were recorded as broadleaf type. Also, the field-based vegetation rapid assessment procedures are subjective and uncertain due to differences in seasonality and surveyors.

A few challenges were encountered in this study, mostly pertaining to uncertainties between the Landsat-derived maps and the reference data. The reference data samples which were utilized during classifier training and testing phases were limited in quantity, and involved positional uncertainty. The bagging method as part of the RF classifier (Breiman, Friedman, Stone, & Olshen. 1984) likely improved the small training data limitation in this study. Another major challenge was the mismatch in time between the available cloud-free Landsat images and the reference data. The GEF reference map was produced four years earlier than the 2011 study period. The field survey (conducted between 2012 and 2015) and the high spatial resolution reference images retrieved from Google Earth and Planet (captured in 2013, 2016, and 2017) are minimally a year apart from the two study periods. This posts difficulty in analyzing the classification products in conjunction with the available reference dataset.

2.6. Conclusions

Frequent anthropogenic disturbances at biodiversity hotspots can degrade ecosystems and ecosystem function. This study demonstrated an effective approach to mapping vegetation cover and land-use utilizing cloud-based image processing tools, even with persistent cloud cover and extreme terrain and illumination effects. A semi-automated mapping approach implemented on an open-access, user-friendly platform, similar to the workflow demonstrated in this study, increases the usability and transferability of such mapping techniques. The use of freely available Landsat imagery and the Earth Engine

image analysis tools ensure that FNNR managers have the resources needed to continue to monitor forest cover and land-use changes. Although future studies will need to continue to improve classification accuracy, particularly for the bamboo/conifer and agriculture classes where mapping errors were higher, this method can be used to evaluate impacts of afforestation policy and identify areas of ongoing human disturbance. With the generalized, four-class maps from multiple dates, land transitions of interest could be identified. For example, areas that were mapped as agriculture before 2001 (prior to PES implementation) and transitioned to bamboo/conifer at a more recent image date could be mapped as locations of PES implementation. These image classification techniques will generate reliable information with regard to forest dynamics (especially in cloud prevalent forested areas like FNNR), which is of great importance not only for assessment of PES efficacy, but also for long-term monitoring and assessment of generic environmental changes or conservation efforts.

Chapter 3. Monitoring Land-Cover and Land-Use Dynamics in Fanjingshan National Nature Reserve

3.1. Introduction

Fanjingshan National Nature Reserve (FNNR) is on the UNESCO World Heritage List because of its high fauna and flora biodiversity, with over 100 endemic species found in the reserve. Roughly 13,000 people live a subsistence life style within the protected area, with a total of 21,000 population within or near the region surrounding FNNR (Global Environmental Facility Project Team, 2004). Human land-use activities such as farming, grazing, and resource gathering take place within or near the reserve (Wandersee, 2013). Frequent anthropogenic disturbances can lead to land-cover and land-use change (LCLUC) and cause ecosystems to degrade quickly, even within designated protected areas (Liu et al., 2001). FNNR has experienced rapid and complex land-use changes in recent years, due to changing demographic patterns, economic and tourism growth, and related development. In 2008, a gondola lift system was built to transport tourists from the east reserve entrance to the FNNR peak. An expanded road network that surrounds the reserve was completed in 2010 (Aitken, An, & Yang, accepted). The last two decades have witnessed increasing outmigration from FNNR to cities as well as rapid initiation and expansion of local off-farm businesses, imposing substantial impacts on FNNR's land use and land cover. Given the wide-spread human activities and the resultant rapid land changes in this pristine, mountainous, and cloud-prone reserve, a closer examination of how to monitor LCLUC in an efficient and reliable manner is important for reserve management.

China has two of the largest payment for ecosystem services (PES) programs in the world (Liu et al., 2008), which aim to increase forest cover and reduce soil erosion and

flooding following the long history of deforestation since the 1960s (Harkness, 1998) and major flooding in 1998 (Uchida, Xu, & Rozelle, 2005). The two main PES programs in China are commonly known as the National Forest Conservation Program (NFCP) and Grain to Green Program (GTGP). The NFCP was implemented in 1998, and the GTGP went into effect in 1999. Under the NFCP regulations, timber harvest would be reduced or even eliminated from natural forests (Liu et al., 2008). The goals are for plantation forests to become the main source of timber harvesting, while natural forests are restored by banning firewood and resource collection. The GTGP policy has a stronger focus on reducing soil erosion by afforestation on sloped land (Uchida, Xu, & Rozelle, 2005; Chen, Marter-Kenyon, López-Carr, & Liang, 2015). Afforestation strategies include planting trees or grass on barren land, converting farmland located on steep slopes (i.e., steeper than 25° in southern China; Xu, Tao, Xu, & Bennett, 2010) to plantation forests. The Chinese government provides payment incentives for both programs. Farmers who enroll in GTGP receive financial and crop compensations, as well as seedlings and technical support for afforestation. The participants of NFCP receive financial support in exchange for forest protection (e.g. patrol and fire watch) and not utilizing forest resources. Both PES programs have been implemented for over 17 years in the FNNR region.

The most feasible and efficient means for monitoring widespread and accelerated afforestation efforts and other LCLUC is through satellite remote sensing. Landsat satellite systems provide a long-term and freely-available image archive which is ideal for land-cover and land-use change monitoring applications. Landsat imagery has the potential temporal frequency of every 16 days and a moderate (30 m) spatial resolution. Reliable change analyses can be achieved with surface reflectance products (Hall, Strebel, Nickson,

& Goetz, 1991; Moran, Jackson, Slater, & Teillet, 1992). Surface reflectance products for Landsat 4 to 7 and Landsat 8 data are processed through automatic algorithms of the Landsat Ecosystem Disturbance Adaptive Processing System (LEDAPS; Masek, 2006) and Landsat Surface Reflectance Code (LaSRC; Vermote, Justice, Claverie, & Franch, 2016) respectively. By converting digital numbers to surface reflectance values, most atmospheric and solar illumination effects are corrected. These corrections enable multi-temporal Landsat images to be more comparable over time.

Different image classification and change identification techniques have been implemented for semi-automated land change studies. A conventional maximum likelihood classifier combined with stable training sites was used to classify nine Landsat image dates for a cloud-prone study area (Stow, Shih, & Coulter, 2014). The technique was deemed effective for long-term LCLUC monitoring. Machine learning type image classifiers were tested by Schneider (2012) with dense Landsat image stacks and training sites of stable and changed features. Among the tested image classifiers, random forest (RF) and support vector machine (SVM) classifiers yielded high accuracies; the RF classifier was found to handle missing image data best. Although machine learning type image classifiers may require larger training samples (Kotsiantis, Zaharakis, & Pintelas, 2007), the RF image classifier was determined by Rodriguez-Galiano et al. (2012) to be less sensitive to small training sample sizes. To quantify land-use changes and retain the transition classes, a post-classification map comparison step was demonstrated by Yuan, Sawaya, Loeffelholz, and Bauer (2005) to be effective.

Several studies have demonstrated the utility of remote sensing to monitoring afforestation in China, though most of them focused on the drier, northern portion of the

country. Zhou and Van Rompaey (2009) utilized SPOT satellite time series images and derived vegetation indices to monitor GTGP in Shaanxi. Significant vegetation cover increase was mapped for the drier portion of their study area, while no vegetation change was detected in the humid and irrigated region. Using Landsat images, Zhou, Zhao, and Zhu (2012) quantified land transitions from agriculture and grassland to afforested land in the semi-arid Loess Plateau area. Their results showed rapid afforestation activity occurred after GTGP implementation and a more fragmented landscape was observed. Landsat time-series images were used to map deforestation and afforestation by Liu et al. (2013) for a 38-year period south of Mongolia. Their highly accurate (89%) results indicated large-scale afforestation activity could be monitored using remote sensing techniques. Spatially extensive and quantitative data about PES distribution and effectiveness in the more humid, southern portion of China remain minimal.

Located in southeastern China, FNNR is a temperate, cloud-prone region with steep terrain and mixed forest cover types, which are great challenges when mapping and monitoring land surfaces using optical remote sensing approaches. Seasonal image composites have been shown to increase the separability of vegetation types and to minimize missing data due to cloud cover (Rodriguez-Galiano et al, 2012; Franco-Lopez, Ek, & Bauer, 2001). Shade and illumination normalization techniques (Wu, 2004; Tsai, Stow, Shi, Lewison, & An, 2016) and spectral vegetation index (SVI) products (Qi, et al., 1994) have been demonstrated to suppress illumination, terrain, and soil reflectance influences. Ancillary data, such as elevation models, were found to improve vegetation classification accuracy (Dorren, Maier, & Seijmonsbergen, 2003; Domaç & Süzen, 2006; Xie, Sha, & Yu, 2008; Belgiu & Drăguţ, 2016). The combined usage of seasonal image composites,

illumination normalization, SVIs, and ancillary data in a previous study mapping vegetation and land-use in FNNR yielded consistent mapping results with moderate accuracy (Tsai et al., 2018).

A software platform that has been instrumental in efficient open-access image processing is Google Earth Engine. Earth Engine (https://earthengine.google.com) is a cloud-based and open-access geospatial data analysis platform (Gorelick, 2017). It provides an image library that can be directly accessed through the JavaScript coding environment. The image library contains data from various sensors and satellite platforms, including almost the entire Landsat image archive and its surface reflectance products. The coding environment allows users to test and implement algorithms and interactively view results. Earth Engine also provides many machine learning type image classifiers for mapping applications. The efficiency of this platform has been demonstrated by Hansen et al. (2013) who generated global forest cover change products from over 650 thousand Landsat 7 scenes in just days. Johansen, Phinn, and Taylor (2015) achieved high mapping accuracies using machine learning image classifiers with Landsat images on Google Earth Engine in a study mapping woody vegetation change. With the readily-available imagery data combined with the open-access image processing capability as Earth Engine provides, forest reserve managers such as those in FNNR, could monitor land change in an extensive manner.

The primary objective of this study is to map, monitor, and quantify land-use transitions pertaining to afforestation and anthropogenic development for the FNNR and its environs. A secondary objective is to assess the utility of monitoring such land-use dynamics in such a challenging cloud-prone and steep terrain study area through Landsat satellite images and Google Earth Engine deploying a workflow previously developed by Tsai et al. (2018).

Vegetation and land-use types are mapped with images captured before and after the PES program implementation in the FNNR region. Techniques such as shade and illumination normalization, and multi-seasonal Landsat image stacks are employed to account for terrain-illumination effects and persistent cloud cover in the study area. Stable training sites are utilized to train a random forest machine learning image classifier to generate vegetation and land-use maps for four periods from 1989 to 2017. Land-use transitions focusing on afforestation and new developments are subsequently mapped. Land-transition maps are examined in conjunction with high spatial resolution satellite imagery to identify corresponding land-use changes.

3.2. Study Area and Data

FNNR in Guizhou province (27.92 N, 108.70 E) was listed as one of the 25 global biodiversity hotspots (Myers et al., 2000). Established in 1978, there are over 5,000 species of plants and animals identified in the reserve. The reserve can be divided into core and buffer zones, totaling about 419 km^2 in size (Yang, Lei, & Yang, 2002). Figure 3 shows the study/mapping area, which includes the reserve core area, the buffer zone, and an area that extends outward by 6 km from the buffer zone to incorporate nearby villages. Forest cover in the reserve core is mostly undisturbed primary forests. The forest composition is complex and mixed. For mapping purposes, the forest community types were generalized based on dominant species into five types: deciduous, evergreen broadleaf, mixed deciduous and evergreen, bamboo, and conifer. Villages and agriculture are found in the surrounding hinterlands of the reserve. These surrounding areas also contain mixed and secondary forests, as well as afforested vegetation from PES programs. Both NFCP and GTGP PES programs are implemented in the FNNR region. The implementation started around year

2001. An estimated 9000 mu (6 km^2) of farmland was enrolled in GTGP for afforestation during 2001-2008 (Wandersee, 2013). About 3 km^2 of land in the reserve were designated as GTGP lands based on a hand-digitized layer created by the reserve staff. In most cases, participants plant pine or fir trees in a mono-crop style. In some occasions, bamboo and economical plants such as tea and fruit trees are also planted.

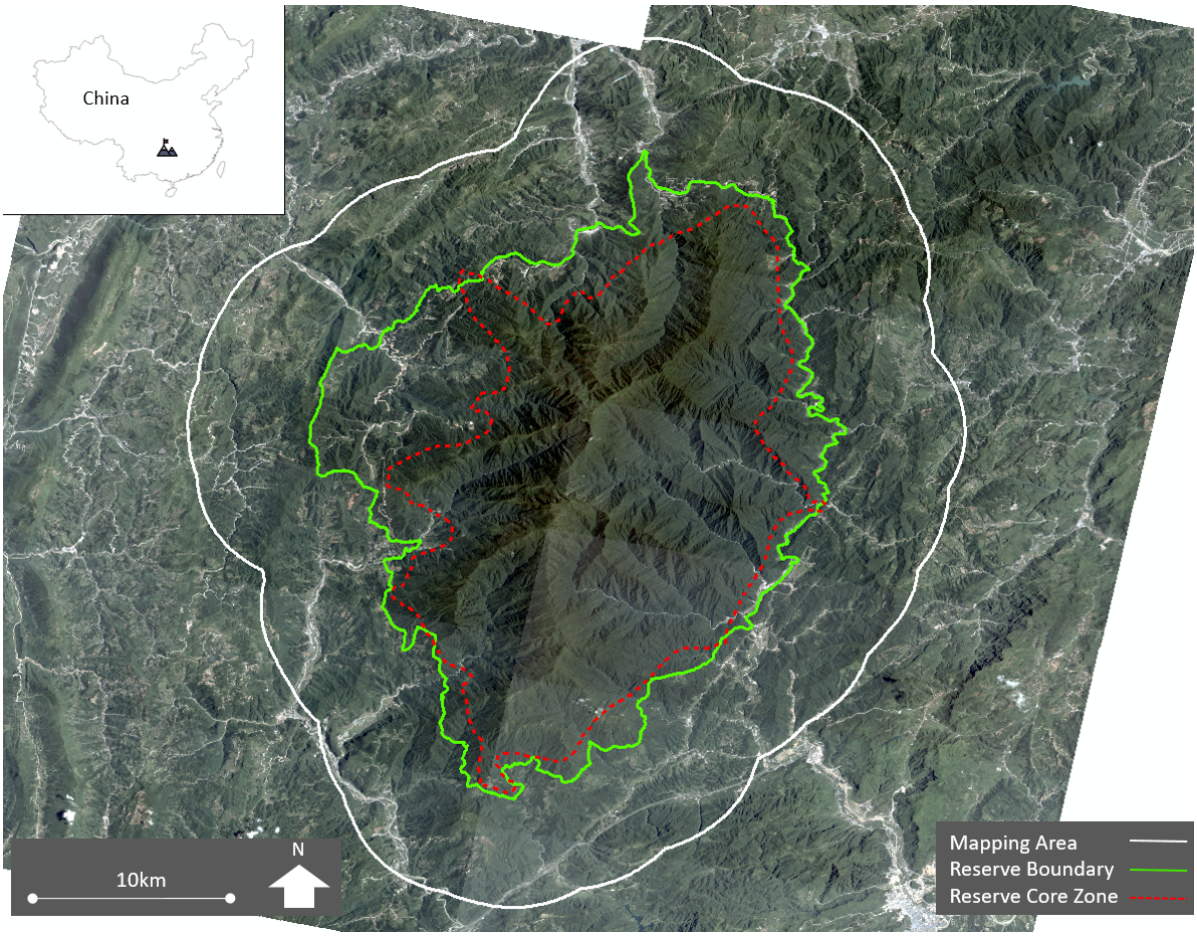

Figure 3. Fanjingshan National Nature Reserve in southeastern China. The reserve boundary is outlined in green, while the reserve core zone in dotted red is slightly smaller. The mapping area (including a 6 km buffer from the reserve boundary) for this study is outlined in white. The backdrop image is a true-color satellite image mosaic collected by Planet Team in July 2017. The mosaicked Planet image exhibits bidirectional reflectance effects but is suitable for visual interpretation.

Available Landsat surface reflectance images that cover the FNNR region (World Reference System 2 path 126, row 41) were identified for the following study periods: Time 1 circa 1989, Time 2 circa 1995, Time 3 circa 2010, and Time 4 circa 2016. Table 6 provides information on specific image dates and number of images used. The four study periods were selected to coincide with and based on (1) the earliest available Landsat data after reserve establishment, (2) prior to and after the GTGP implementation in the region in 2001, and (3) the most up-to-date land-use and land-cover. A four- and six-year image cycle was found to be appropriate to monitor anthropogenic-related vegetation changes (Coppin & Bauer, 1995), and a ten-year interval was found sufficient to transition from successional vegetation to forest (Park, Houghton, Hicks, & Peterson, 1983).

Table 6. Image dates and number of images associated with the study periods for this study.

Study Period	Sensor	Seasonal Composite Images	Number of Images
Circa 1989	**Landsat 5**	1989-1990	12 images
Circa 1995	**Landsat 5**	1995-1996	12 images
Circa 2010	**Landsat 5**	2010-2011	11 images
Circa 2016	**Landsat 8**	2016-2017	17 images

A digital elevation layer from the Shuttle Radar Topography Mission (SRTM) was incorporated in the classification workflow. C-band and X-band data were collected with different antenna panels for SRTM in the year 2000 (Farr, 2007). The C-band derived digital elevation model (DEM) has near-global coverage and was processed by NASA JPL. The one arc-second (roughly 30 m) spatial resolution topographic data were released for public use in 2015.

Some high spatial resolution satellite imagery data were available for viewing, and were utilized during the analysis. Imagery data include true-color Pleiades images from 2013 and 2017 on Google Earth, and pan-sharpened QuickBird/GeoEye/WorldView-2 mosaic images

from 2004 to 2012 available as Basemap in the ArcGIS software. Four-band Planet images (red, green, blue, and near-infrared bands) were made available through its Education and Research Program (Planet Team, 2017). Two cloud-free mosaicked products were generated from Summer 2016 and Summer 2017 for the FNNR study area. The mosaicked image set exhibits bidirectional effects, however it is suitable for the visual interpretation purposes.

3.3. Methods

Vegetation and land-use types were mapped for each of four study periods and the resultant maps were assessed for accuracy. Then land-transition maps were generated through post-classification map comparison to emphasize lands that underwent afforestation and development of new built land cover.

3.3.1. Classification Feature Input

Landsat surface reflectance images for each study period were first compiled into seasonal composites (Refer to Table 6 for the number of images used to create the seasonal composite for each study period.) A mean value composite image was generated for each season group before they were layerstacked for each study period. Several types of SVI image sets were derived for each season group and image date, for subsequent input to image classifiers. Several types of SVI image sets were derived for each image date, for subsequent input to image classifiers. The indices were meant to enhance vegetation and soil moisture signature, and suppress terrain illumination differences. These included normalized difference vegetation index (NDVI; Carlson & Ripley, 1997), modified soil adjusted vegetation index (MSAVI; Qi et al., 1994), normalized difference blue and red (NDBR), normalized difference green and red (NDGR), normalized difference shortwave infrared and

near infrared (NDII), and spectral variability vegetation index (SVVI; Coulter et al., 2016). MSAVI and NDVI are calculated as defined in Equations 1 and 2 of Chapter 2. NDBR, NDGR, and NDII are calculated as the form of NDVI using blue and red bands for NDBR, green and red bands for NDGR, and infrared bands (NIR and SWIR) for NDII. SVVI is calculated as the pixel-wise difference between standard deviation (SD) of all Landsat bands (excluding thermal) and SD of all three infrared bands, as defined in Equation 3 of Chapter 2. Elevation, slope, and aspect were generated from the SRTM DEM layer, and layerstacked with the seasonal SVIs as the classification feature input for vegetation and land-use mapping.

3.3.2. Image Classifier Training Data

The classification scheme consists of five common forest types in the area, including deciduous, evergreen broadleaf, mixed deciduous and evergreen, conifer, and bamboo, plus three land-use classes: built, agriculture, and bare. A total of 120 single-pixel training samples were extracted and compiled through vegetation type survey and manual image digitization. When available, stable training pixels (Gray & Song, 2013; Shih, Stow, Weeks, & Coulter, 2016) representing a known vegetation or land-use type for the duration of the study period were utilized to classify all four study periods. Through vegetation type survey during Spring 2015, Fall 2015, and Spring 2016 in FNNR, a total of 84 plots that are 20-by-20 m or 30-by-30 m in size were recorded for the five dominant forest types based on accessibility on the ground. These plot locations were cross-referenced with cloud-free Spring Landsat imagery to ensure the forest cover were present in all study periods. Eight out of the 84 forest point samples were found to transition from agriculture to conifer forest between c. 1989 and c. 2016 due to PES implementation. These eight samples were recorded

as agriculture class for the first two image dates, and conifer class for the latter two image dates. The remaining 76 samples manifested as stable forest type from the first image date to the last.

For the built, agriculture, and bare land-use classes, a total of 36 stable training pixels were manually selected using the approach similar to what Stow, Shih, and Coulter (2014) have used. The first image date was used as the basis for selecting built training samples. The latter Landsat image dates were used to generate initial agriculture training samples, based on the rationale that agriculture lands were persistent during the study period if afforestation was not observed. The sample pixels were cross-referenced with the 1989 Landsat image date to ensure stability. Training sample pixels were ensured to locate within a homogeneous portion of the image (i.e. within a single vegetation or land-cover type). The training dataset included 33 samples of mixed forest, 12 broadleaf forest, 9 deciduous forest, 10 conifer (18 for 2010 and 2016), 12 bamboo, 15 agriculture (23 for 1989 and 1995), 15 built, and 6 for bare ground.

3.3.3. Classification, Post-Processing, and Post-Classification Change Analysis

A pixel-based, supervised RF machine learning image classifier was used to generate vegetation and land-use maps for each of the four time periods. The 120 training samples were randomly selected and split into two-thirds and one-third portions respectively for training and testing the image classifier (i.e., cross-validation). A grid search was performed by exhaustively testing combinations of parameters to identify the optimal RF classification parameters—number of trees and number of variables per split. The vegetation and land-use maps were generated with the parameters that yielded the highest testing accuracy. The maps were smoothed with a 3-by-3 pixel majority moving window to minimize mixed-pixel

and boundary effects on misclassification, and to generalize to a more realistic minimum mapping unit.

Land-use transition maps were generated through a post-classification comparison approach (Jensen, 1996) to depict afforestation and new built development based on the Landsat-derived vegetation and land-use maps. Logical land change rules were applied such that afforestation activity and new built developments could be mapped with pixels that transitioned from-to classes of interest. To map afforestation activity, pixels that were mapped as agriculture in the earlier study periods and as conifer in the third or fourth study periods were labeled as afforested land. New built development was identified for pixels that were mapped in an earlier image date as any non-built classes (forest, bamboo/conifer, and agriculture) and then as built in a later image date.

3.3.4. Map Accuracy Assessment

Map accuracy was assessed for the four dates of vegetation and land-use maps, as well as the land-use transition maps. The vegetation and land-use maps were assessed for mapping accuracy using an independent set of 128 accuracy assessment point samples. The samples were created in a random sampling manner with a distance restriction (points to be minimally five Landsat pixels apart) and are dispersed within the entire mapping area. Samples were labelled manually using the 3 m spatial resolution Planet imagery captured in July 2017 (Planet Team, 2017). These samples represent four vegetation and land-use classes, 32 points per class: forest, agriculture, built, and bamboo/conifer. To keep the analysis consistent, the vegetation and land-use maps were also categorically aggregated or generalized. The deciduous, evergreen broadleaf, and mixed deciduous and evergreen classes were grouped and recoded as forest; bamboo and conifer classes were merged as a

single bamboo/conifer class representing PES afforested lands; agriculture and built remained separate. The accuracy assessment samples were compared to the corresponding image pixels on the generalized maps. Mapping agreement, producer's, user's, and overall accuracies were recorded.

Accuracy of the land-use transition map was assessed in a more qualitative manner due to a lack of available high spatial resolution reference imagery that corresponds to the earlier study periods. Centroids of 24 PES afforested lands were recorded through field visits in FNNR during Spring 2018 and then verified on high spatial resolution satellite imagery on Google Earth. The Landsat-derived afforestation maps were compared to the 24 PES reference points to evaluate the afforestation mapping results. The new built maps were visually inspected in conjunction with high spatial resolution satellite imagery from ArcGIS Basemap, Planet imagery, and Landsat images to identify and label the specific type of land-use changes.

3.4. Results

3.4.1. Vegetation and Land-Use Map Accuracy

The four-class vegetation and land-use maps have overall accuracies ranging from 64 to 79% for the four study periods. Table 7 and Table 8 show the accuracy assessment results for before and after PES implementation respectively for the four study periods. The earlier two study periods have moderate mapping accuracies at 64 and 69% for 1988 and 1995 respectively, as shown in Table 7. As seen in Table 8, maps for the latter two (more recent) study periods have higher overall accuracies of 77 and 79% for 2010 and 2016 respectively. Of the four classes, forest and built were consistently classified with high accuracies. Greater mapping confusion occurred for agriculture and bamboo/conifer classes. These land-

cover and land-use types are likely under-classified, as indicated by the lower producer's accuracies and higher user's accuracies. The aggregated bamboo/conifer class is often confused with forest, while agriculture is confused with built.

Table 7. Accuracy assessment results for the c. 1989 and c. 1995 (i.e., prior to PES implementation) classification products generated with the seasonal composite image input and random forest classifier. These values were derived using the final accuracy assessment data on the four-class generalized map. Gray cells indicate agreement.

Image-derived Class	**Reference Class**								**User's Accuracy**	
	Forest		Agriculture		Built		Bamboo & Conifer			
	1989	1995	1989	1995	1989	1995	1989	1995	1989	1995
Forest	28	27	7	6	8	3	10	10	53%	59%
Agriculture	1	1	15	18	3	3	3	3	68%	72%
Built	0	0	10	6	21	25	1	1	66%	78%
Bamboo & Conifer	3	4	0	2	0	1	18	18	86%	72%
Producer's Accuracy	88%	84%	47%	56%	66%	78%	56%	56%	Overall Accuracy	
									64%	69%

Table 8. Accuracy assessment results for the c. 2010 and c. 2016 (i.e., post-PES implementation) classification products generated with the seasonal composite image input and random forest classifier. These values were derived using the final accuracy assessment data on the four-class generalized map. Gray cells indicate agreement.

Image-derived Class	**Reference Class**								**User's Accuracy**	
	Forest		Agriculture		Built		Bamboo & Conifer			
	2010	2016	2010	2016	2010	2016	2010	2016	2010	2016
Forest	30	29	3	0	0	0	9	10	71%	74%
Agriculture	0	0	17	24	2	0	0	3	89%	89%
Built	0	0	11	4	30	31	2	2	70%	84%
Bamboo & Conifer	2	3	1	4	0	1	21	17	88%	68%
Producer's Accuracy	94%	91%	53%	75%	94%	97%	66%	53%	Overall Accuracy	
									77%	79%

3.4.2. Land Change Maps and Distributions

Afforestation and new built developments were mapped between 1995-2010, and 1995-2016. Distributions of afforestation and new built developments were also examined for these two periods. The 1989 date was excluded because of its relatively low agriculture mapping accuracy. Figure 4 shows afforestation land mapped for 1995-2010. Mapped afforested lands are located mostly near the reserve boundary, particularly alongside river

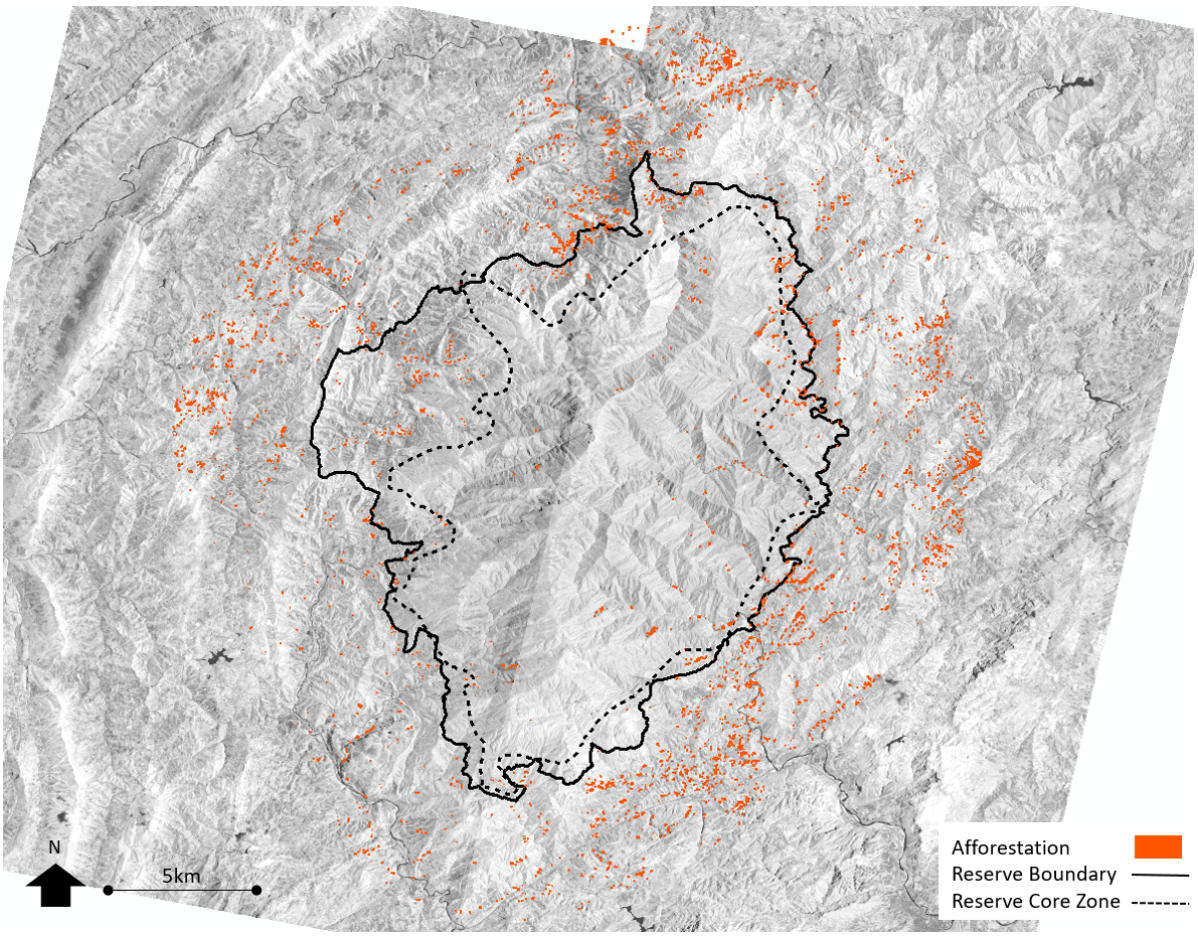

Figure 4. Map of afforested lands in Fanjingshan National Nature Reserve from 1995-2010 overlaid on a Planet gray-scale NIR image mosaic. Afforestation is mapped from pixels transitioned from agriculture to conifer/bamboo class. The mosaicked Planet image displayed bidirectional effects but remains suitable for visual interpretation.

channels, roads, and valleys and creeks that originated from the reserve core. Similar distribution patterns were observed in both 1995-2010 and 1995-2016 afforestation maps. However, the 1995-2016 afforestation map portrays substantial errors in the area to the east of the reserve. This region, approximately 2 km^2 in size, remained mostly agriculture from 1995 to 2016, while the 2016 map portrayed it as conifer. This was likely a result of the lower mapping accuracy of bamboo/conifer class, and the under-classification of agriculture from the 2016 image date. In 15 out of the total 24 recorded PES reference locations, afforestation areas are mapped within a three Landsat pixel radius (90 m).

Figure 5 shows the new developments mapped between 1995-2016. Many new built developments are mapped along the reserve boundary and river channels in a linear pattern. In the adjacent reserve environs, new built developments are mostly clustered in nearby towns and villages. While the road networks were mapped more contiguous in 2010 than in 2016, the 2010 map misclassified agriculture land as built in many instances. Indicated by the accuracy assessment result shown in Table 8, the 2010 map likely had an over-classified built class and an under-classified agriculture class that led to more area being mapped as new development in the transition maps.

The new built maps reveal that development in the study area corresponds to widening, paving, and building of roads and freeways, building of tourism and recreational infrastructure, and developing of villages and other infrastructure. Figure 6 shows examples of the mapped new built developments in detail. Some of the recreational developments that were mapped correspond to the construction of a golf facility and the station for the gondola lift as seen in Figure 6a and 6b respectively, both located on the east side of the reserve. The

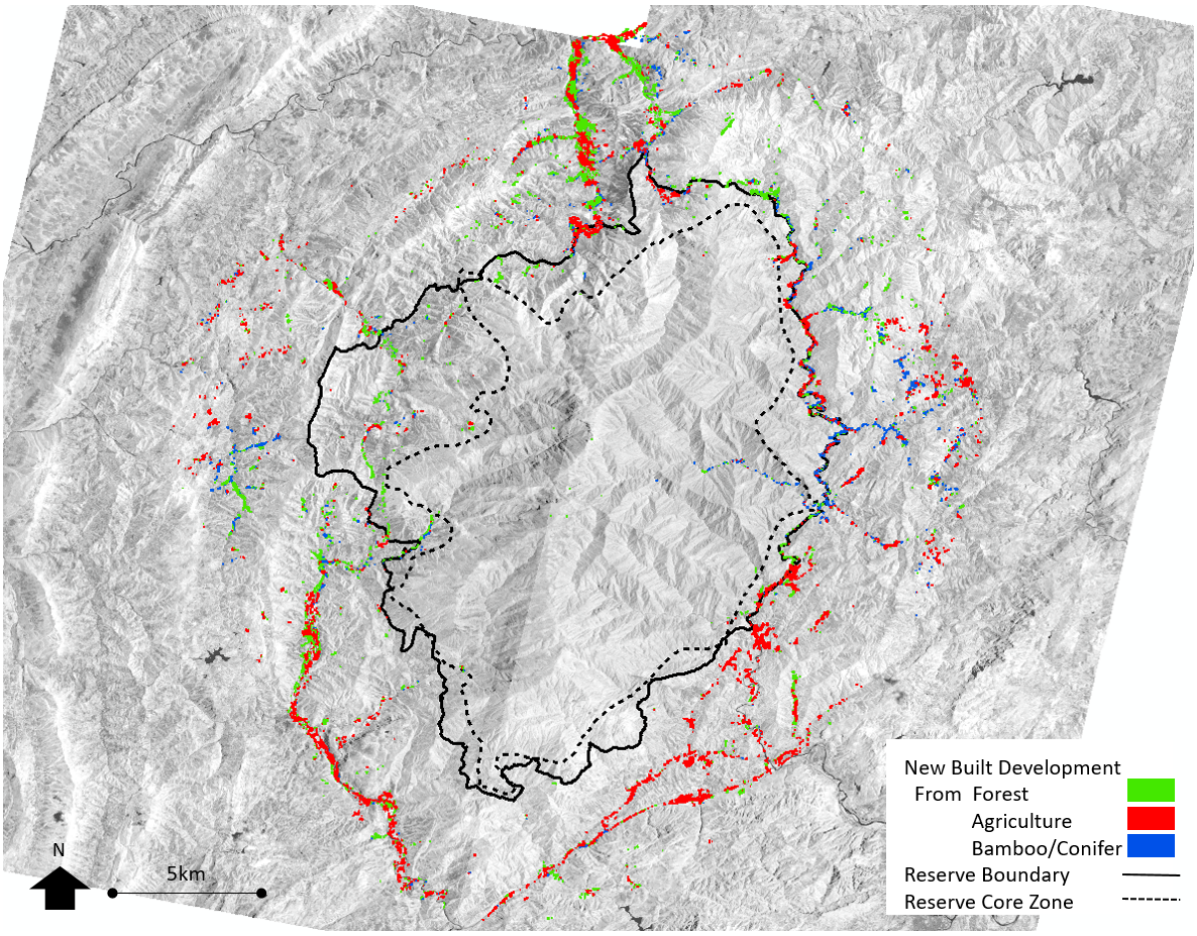

Figure 5. New development map from 1995-2016 overlaid on gray-scale NIR Planet image mosaic in Fanjingshan National Nature Reserve. New development was identified by pixels transitioned from forest, agriculture, or conifer/bamboo (represented by different colors) to the built class. The mosaicked Planet image displayed bidirectional effects but remains suitable for visual interpretation.

gondola lift station is slightly larger than one Landsat pixel (30-by-40 m) in size, while the golf course is roughly .4 km^2 in size. Other mapped infrastructure development primarily corresponds to the following types of construction activities and features: (1) building of freeways south and west of reserve as Figure 6c shows; (2) completion of the road network surrounding the reserve; (3) constructing of new roads to connect villages, mostly north and northwest; (4) constructing two dams to the west (Figure 6d illustrates one of them); (5)

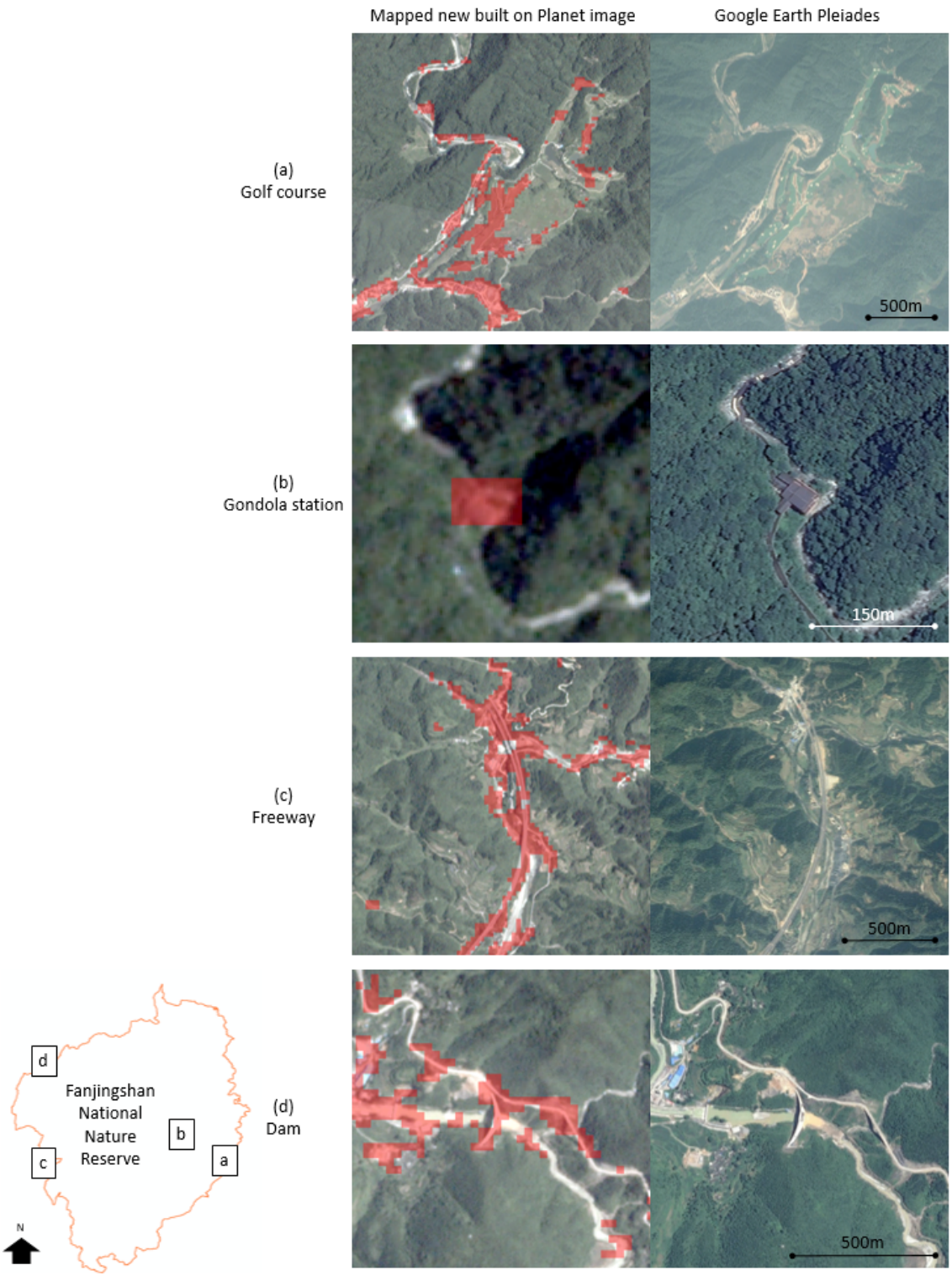

Figure 6. Examples of mapped new built development (shown in red) in Fanjingshan National Nature Reserve between 1995 and 2016 overlaid on Planet true-color mosaic image and a Pleiades image from Google Earth: (a) a golf course located to the east of the reserve; (b) a gondola station within the reserve; (c) part of a freeway network to the west of reserve; and (d) a newly-constructed dam also to the west.

developing tourism infrastructures such as reserve entrances on both east and west side of the reserve; and (6) building a sports field at a nearby town to the east.

To improve the reliability of the land transition maps, manual editing was performed to remove the apparent transition errors. Pixel groupings incorrectly classified as new built development due to the misclassified agriculture and built classes were recoded for the new built development maps. Falsely mapped afforested pixels due to misclassified agriculture and bamboo/conifer classes were also recoded for the afforestation maps. The areas of afforestation and new developments are summarized based on the mapped and edited land transition maps. Table 9 shows the quantified area of afforestation and new development for 1995-2010 and 1995-2016. Approximately 10 and 12 km^2 of the study area was mapped as afforestation based on the 1995-2010 and 1995-2016 land transition maps, respectively. Most of the afforestation activity occurred outside of the reserve, as only 1.33 and 1.45 km^2 of afforestation were mapped within the reserve boundary (i.e., core and buffer zones).

Table 9. Mapped new built development and afforestation area for 1995-2010 and 1995-2016 periods. Areas are measured for the FNNR core zone, the entire reserve, and the reserve plus the 6 km surrounding environs. Areas are measured in km^2.

Mapped Area (km^2)	Reserve Core	Reserve	Reserve & Environs
2010 New Built	0.47	3.89	37.72
From Forest	0.30	2.08	14.18
From Agriculture	0.05	0.94	16.11
From Bamboo/Conifer	0.12	0.87	7.43
2010 Afforestation	0.49	1.33	10.09
2016 New Built	0.25	1.90	25.06
From Forest	0.09	0.92	8.33
From Agriculture	0.04	0.55	13.55
From Bamboo/Conifer	0.12	0.42	3.18
2016 Afforestation	0.16	1.45	12.46

A substantial amount of development occurred during the study period based on the new development maps. A total of 25.06 km^2 is mapped as new development from 1995 to 2016. Over 37 km^2 of the study area was portrayed as new development between 1995 and 2010.

Relatively little development occurred within the protected area, as seen in Table 9 and depicted in Figure 5. Less than 4 km^2 are mapped as new built development within the reserve boundary, and less than 0.5 km^2 within the core area. Among the observed new built developments within the reserve are small-scale land transitions corresponding to road construction along the valleys on the east and west side, and the recreational/tourism developments (namely reserve entrances, the gondola lift station, and the tourism infrastructure at the reserve peak). The majority of the new development is found outside, but adjacent or leading towards the reserve. The golf facility and a tourism attraction of a local indigenous tribe were both established within 1 km of the reserve boundary. Over 33 and 23 km^2 new development were mapped in the reserve environs for 1995-2010 and 1995-2016 respectively. Table 9 also reveals that forest was the most common type to transition to built within the reserve area, while agriculture land experienced the most land conversion to built outside of the reserve.

3.5. Discussion and Conclusions

Long-term monitoring of LCLUC in nature reserves is important worldwide given human induced, widespread degradation of ecosystems (Vitousek, 1994) and the corresponding ecosystem services vital to human being (Daily & Matson, 2008). Such monitoring is also pivotal to assess the efficacy of PES programs in China, which has experienced wide-spread, PES-related afforestation while subject to relatively rapid infrastructure development at the same time. In this study, sporadic development and land-use changes were found in the core FNNR area, and more extensive land-use changes in the buffer zone and its adjacent environs between 1995 and 2017 that coincided with the implementation of PES programs.

The quality of the Landsat-derived vegetation and land-use maps and their associated mapping accuracies are generally consistent and suitable for land change monitoring. No terrain effects or cloud artifacts are apparent in any of the Landsat-derived maps. The vegetation type distribution was mapped in a mostly consistent manner throughout the study periods. The c. 2010 and c. 2016 study periods yielded higher classification accuracies compared to the two earlier dates. This could be attributed to the higher quality Landsat images and reference data used for training and accuracy assessment. Seventeen images with acceptable cloud cover were available and incorporated in the seasonal composite for the c. 2016 period, yielding the highest classification accuracy of all four dates. The composites for 2010 and 2016 (later) years are comprised of more summer images that capture the fully leaf-on vegetation signature. For c. 2016, 11 summer images were utilized compared to five for each of the first two dates. The classification training data were derived based on field surveys and images that corresponded more closely with the latter image dates in time. Although training pixels were examined on c. 1989 and c. 1995 Landsat images and evaluated for stability, greater uncertainty exists with over 20 years of temporal difference in the reference data. Available training data are limited for training the RF machine learning image classifier due to limited access posed by dense vegetation and steep terrain in the study area. These samples are not well-distributed and likely do not encompass the full spectral signature variability of the mapping classes.

Most newly developed and many afforestation areas were correctly identified and mapped. However, mapping errors from the earlier two study periods due to the misclassification of agriculture land and conifer/bamboo vegetation are manifested in the afforestation and new built development products. Accurate vegetation and land-use

mapping was challenging because of the complex and mixed forest composition and agriculture planting style in the study area. The composition of mixed vegetation cover in the reserve consists of various degrees of conifer, bamboo, evergreen broadleaf, and deciduous forest due to the humid, temperate climate and the steep terrain and elevation gradient. This likely led to the under-classification of conifer and bamboo, and their confusion with the mapped forest class. Bamboo and conifer naturally grow in the region and are often found on the edge of disturbed agriculture land. Agriculture in the FNNR region occurs mostly as small-scale subsistence farming on steep slopes and terraces. Crop types were mostly leafy greens that are small and low in stature, planted sparsely with secondary vegetation mixed in and a lot of soil exposed. The agriculture planting style likely led to a similar spectral signature of high reflective bare or impervious surface especially on the moderate spatial resolution Landsat pixels, and caused the classification confusion with the built class. The farming cycle followed the seasons closely. During winter, agriculture land was mostly bare. This planting pattern is likely why agriculture is sometimes confused with deciduous forest cover. Improving the mapping accuracy, particularly for the subsistence agriculture, can increase the reliability of the derived land transition products and the applicability to other regions of similar land-use types.

Open-access and web-based Google Earth Engine software offers a powerful image processing platform. The cloud-computing capability of the Google Earth Engine platform makes it simple and efficient from compositing multi-temporal imagery to implementing machine learning image classification routines to generating results. The coding environment allows users to streamline image processing workflow. Its inclusive raster processing functions can be easily implemented using JavaScript, with guidance from

documentation and tutorial resources. The platform requires a valid Google user account and a simple online application to access. Compared to many commercial image processing software packages, there is no license or maintenance fees attached to Earth Engine (for education, research, and non-profit users), and it does not require downloading or installing software packages. However, access and performance of Earth Engine is limited when an internet connection is not available or unstable. Viewing and evaluating results with commercial image processing software (e.g., ERDAS IMAGINE or ArcGIS) was more efficient. Manipulating displays of images and maps is simpler and more efficient when the data are stored locally on the computers. The platform also lacks manual editing capabilities. Regardless, implementing and executing the workflow on Google Earth Engine after the methods were finalized is beneficial for reserve managers in many ways. The streamlined workflow minimized personnel training and the open-access platform eliminated the costly hardware and software.

The original attempt to monitor forest cover change as a means of evaluating conservation efforts in FNNR was through Landsat-derived canopy fractional cover mapping (CFC; Tsai, Stow, Shi, Lewison, & An, 2016). Canopy fraction represents the amount of canopy closure as a percentage of each image pixel area occupied by tree canopy (Wang, Qi, & Cochrane, 2005). Continuous CFC data can more precisely represent forest cover variations in complex landscapes (Hansen, 2003), and its magnitude change can reflect the degrees of forest cover change related to degradation, thinning, and clearing. While results suggested that the modeled CFC changes were likely due to anthropogenic activities, the accuracy of the CFC estimates was uncertain. Ground-based estimation of canopy closure was derived through a commonly used digital hemispherical photography

technique (DHP; Pueschel, Buddenbaum, & Hill, 2012), and substantial variability in correspondence was found between the ground-based and Landsat-derived CFC values, though range and median CFC were similar throughout the areas for which ground-based estimates were made. This could be attributed to the positional uncertainty of ground-based DHP data, and differences in view perspective. The dense canopy in steep terrain likely limited the positional accuracy of the satellite positioning device used to record the DHP data locations. The understory of dense green vegetation provides a low contrasting background, unlike using the up-looking ground-based technique where tree cover contrasts well against a blue sky or cloudy background. The majority of land change in FNNR is observed to associate with land use conversion, such as agriculture abandonment, afforestation, and new built expansion, rather than forest thinning and cutting. Mapping multi-temporal vegetation and land-use types was determined suitable for the purpose of environmental monitoring.

It is worth noting that cash crops like tea and fruit trees are also planted as part of the GTGP implementation in FNNR, though they are limited to several selected villages. Tea bushes planted under the guise of PES were observed in a small village to the northwest of the reserve, on terraces surrounded by conifer stands. Small plots of yellow peaches and pears planted in the southern region were observed, both planted sparsely on terraces and mixed in with secondary regeneration after year 2016. The areas where tea and fruit trees are grown are mapped mostly as agriculture in all four image dates, with some bamboo/conifer cover or mixed forest within. Tea or fruit tree orchards were not incorporate into the classification scheme, as they are not common nor well distributed within the study area.

Despite the recognized importance of mapping and monitoring vegetation and land-use changes in an era of many global changes arising from or related to rapid population growth, over exploitation of natural resources, and the related environmental degradation (Ripple et al., 2014), this task remains challenging for cloud-prone and mountainous areas, such as FNNR. The combined techniques of utilizing seasonal image composites, applying illumination normalization, and incorporating ancillary data facilitated reliable mapping of land cover and land use for forest reserves characterized by steep terrain and high cloud cover. The implementation of stable training samples and logical land-use transition rules generated reasonably accurate land-use maps for a period of over 26 years. Future studies could focus on improving the mapping accuracy by increasing the training sample size and increasing the usability of the image processing workflow by integrating the Earth Engine code into a web application with a graphical user interface. Yeh (2009) and Feng et al. (2005) indicate that farmers show intentions to return to farming once the PES compensation ends. PES land was also associated with lower wildlife species richness (Chen et al., in review). The mapping approach and land-use transition maps demonstrated in this study could provide extensive insight into locations of afforestation and build development lands. More extensive monitoring of land-use conversion is also important for evaluating mid- to long-term ecological impacts of PES and other conservation programs, such as afforestation outcomes, reduced soil erosion, slope stability, and runoff.

Chapter 4. Monitoring Forest Cover Change Within Different Reserve Types in Southern Ghana

4.1. Introduction

Forest cover is associated with ecosystem services that are vital to human health and livelihoods, including watershed protection, climate change mitigation, and soil erosion prevention. However, tropical forests globally were depleted at an annual rate of 6 million hectares in recent years, while agriculture land increased by almost the same amount, based on a report by the Food and Agriculture Organization of the United Nations (FAO, 2016). Other studies indicate that most of the deforestation in tropical forests is related to agricultural practice (Barraclough & Ghimire, 2000; Appiah et al., 2009; UNEP GEO-5 report, 2012). Population dynamics have also been commonly associated as an underlying and indirect cause for deforestation, particularly in rural regions (Carr, 2004; Carr, Suter, & Barbieri, 2005). Ghana, as a developing country in sub-Saharan Africa, has experienced steady economic, population, and urban growth, and in turns, land-cover and land-use change. The country's total population increased from 19 million to 25 million between 2000 and 2010 (Ghana Statistical Service, 2012). Ghana's GDP had an annual gain of 6.6% from 2010 to 2014 (FAO, 2016). Despite net rural-to-urban migration and over half of the population resides in urban areas since 2010, rural population continues to grow, suggesting that fertility rates remain high (FAO, 2016).

4.1.1. Forest Resources and Deforestation in Ghana

Most of the pristine forest resources, including tropical evergreen seasonal forest and tropical semi-deciduous forest (UNESCO, 1973), are located in the high forest zone in the

southern part of Ghana. These primary forests in Ghana are mostly depleted due to agricultural expansion and over-exploitation of forest resources (Appiah et al., 2009). Timber, surface mining, and export-oriented agriculture are among the main economic activities in Ghana (Hens & Boon, 1999), and these activities are destructive to forest cover (Osafo, 2005). Heavy logging activity took place during the 1960s and 70s in Ghana. Almost all forests, even within protected areas, have been selectively logged at some point of time, and many of them since 1990. Vegetation outside of the reserves is mostly secondary regeneration on abandoned farms (Hall & Swaine, 1976; Dickson, Benneh, & Essah, 1988), with small agricultural plots mixed in. Expansions of plantations of trees, oil palm, and cocoa also contribute to deforestation or forest degradation. The commonly practiced taungya system, in which plantation workers are given rights to grow agriculture crops among forest plantations, can cause forest disturbances (Kalame et al., 2011; Hawthorne & Abu-Juam, 1995). Unsuccessful taungya systems can lead to forest cover conversion to agriculture; this "slash-and-burn" agriculture practice can also lead to higher fire risk within plantations and forests. Ghana is a major producer of gold, bauxite, and manganese among African countries. In 2016, its total gold output was over 113400 kg. Twenty-three large-scale mines were located in the country in 2016 and most of them operate as open pit mines. This surface mining style and mine expansions cause both large- and small-scale forest cover removal.

It is estimated by the FAO that the livelihood of 2.5 million people in Ghana depends on forests. Appiah et al. (2009) documented that almost 40% of rural household income in Ghana consists of forest-related activities. More revenue is generated and more forest is cleared when the household is larger or resides closer to forests. With a lack of off-farm

work opportunities, rural residents rely on poverty-driven agriculture (compared to economical, longer-cycle planting). Short cycle crops are planted and shifted between agriculture plots while long cycle crops are also cultivated. This practice generates higher crop yields, but is also destructive to forest cover (Barraclough & Ghimire, 2000). Firewood collection from fields and forest near villages is also common in rural regions (Calvo, 1994). Firewood is the preferred and main fuel source for cooking, and few households use charcoal or crop residue according to the Ghana 2010 population and household census (Ghana Statistical service, 2012). Due to deforestation, the travel time and distance to collect firewood have increased in recent years according to an UN report (2010).

Individuals and local communities/tribes own roughly 80% of the lands in Ghana. Most of these customary lands are managed based on tribal customary laws and not bound by specific national management laws (Ubink & Quan, 2008). The remaining 20% of lands in Ghana are state owned, which the Ghanaian government owns and manages. Over 200 forest reserves and protected areas (i.e., on-reserves) are set aside to be managed by the Ghanaian government (Osafo, 2005) and they are located on both customary land and state land. However, reserves are further classified with different protection status and human disturbances are still present. Protected areas are classified as conversion, production, and protected reserves (Hilson & Nyame, 2006). Conversion reserves are degraded regions that are being targeted for replanting. Production reserves are resource reserves that can be used to sustainably produce wildlife products, timber and non-timber products, used for cultural practices (e.g., tribal sacred lands), tourism, and trophy hunting (Hawthorne & Abu-Juam, 1995). Protected reserves, including national parks, allow no exploitation. However, based on a management evaluation report published by the International Union for Conservation of

Nature (Hawthorne & Abu-Juam, 1995), even protected reserves and national parks can experience land conversion, bush fire, and encroachment.

4.1.2. Remote Sensing Solutions to Monitoring Land Change in Cloud Prone Areas

Remote sensing offers a cost-effective and practical means to map vegetation, other land cover and land use over large areas, compared to field survey. Moderate spatial resolution satellite systems such as Landsat provide near-global coverage of multispectral imagery dating back to the mid-1980s that can be used to monitor long-term and extensive forest cover. Landsat surface reflectance products offer more comparable and reliable land change analysis than spectral radiance or digital number products (Hall, Strebel, Nickeson, & Goetz 1991; Moran, Jackson, Slater, & Teillet, 1992). These surface reflectance products are generated by algorithms implemented by the Landsat Ecosystem Disturbance Adaptive Processing System (LEDAPS; Masek et al., 2006) for Landsat 4 to 7 imagery, and Landsat Surface Reflectance Code (LaSRC; Vermote, Justice, Claverie, & Franch, 2016) for Landsat 8 images.

Optical satellite imagery can be susceptible to cloud cover, particularly in humid and tropical regions where cloud cover and optically thick atmospheres are predominant. Much research has demonstrated the potential of dense image composites, formed by combining multi-temporal cloud-free observations, to resolve cloud cover and cloud shadow issues (Broich et al., 2011; Huang et al., 2009; Hansen et al., 2008). Lindquist, Hansen, Roy, and Justice (2008) evaluated pixel quality for humid tropics in central Africa and found that ideally, all available image data would be utilized to achieve the highest image composite quality. Coulter et al. (2016) utilized dense Landsat images to derive maximum value image composites as a means to resolve the frequent cloud cover and cloud shadow issue in

southern Ghana. Their derived land cover and land use change map detected changes with over 70% accuracy, although some image anomalies from maximum-value compositing were present. Ruefenacht (2016) tested the utility of median value image composites to estimating tree canopy percent cover. Median value composites were found to retain comparable image information and yielded less image anomalies from cloud and shadow pixels compared to the maximum value composite products, as median value is more resistant to data outliers. The utility of median value image composites is tested in this study of southern Ghana.

Unsupervised image classification or clustering followed by manual labelling is commonly adopted for large area land-cover mapping, particularly when the mapping classes are uncomplicated (Franklin & Wulder, 2002) or when training data are not readily available for supervised image classifiers, such as the machine learning type implemented in Chapters 2 and 3. Muller, Racoviteanu, and Walker (1999) mapped tundra and shrublands in northern Alaska with multiple scenes of Landsat images using K-means clustering. The derived map yielded 87% mapping accuracy. Forest and meadow were discriminated using Landsat imagery and ISODATA clustering in Yellowstone by Debinski, Kindscher, and Jakubauskas (1999). Unsupervised image classification techniques have also been applied to map land-cover and land-use in Ghana. Pabi (2007) utilized Landsat TM images and ISODATA clustering to map land-cover and land-use for eight sites within two census districts in central Ghana. With a post-classification map comparison between 1991 and 2001, Pabi found that dense woodland area decreased significantly in all eight sites while cultivated land increased. The effectiveness of unsupervised image classification has not yet

been tested in mapping the extensive tropical southern Ghana region where cloud cover is prevalent.

Land-cover and land-use change in Ghana has been examined in previous studies based on remote sensing data and techniques, mostly for localized areas. Forest cover decrease and concomitant increase in other land uses (e.g., built, agriculture, and mining area) are common findings in these studies. Kusimi (2008) mapped land-cover and land-use change of 1986-2002 within a single census district in southwestern Ghana, using Landsat TM images and a combination of unsupervised and supervised image classification routines. He found that forest reserves in the district experienced significant forest cover loss of over 400 km^2, while areas of mining, farming, built, and population in the district increased. Yorke and Margai (2007) mapped land-cover and land-use for 1990 and 2000 Landsat images using a supervised, Maximum Likelihood image classification routine for a watershed in southeastern Ghana. They found forest cover decreased by over 32%, while agriculture land and built expanded substantially. Coulter et al. (2016) mapped land-cover changes between circa 2000 and circa 2010 using four Landsat scenes covering much of southern Ghana, and found that 62% of the land changes were related to agriculture land increase. An up-to-date and more extensive examination on forest cover change in southern Ghana is needed and can aide in land-use decisions and conservation efforts.

The objectives of this study are twofold. First, land-cover and land-use changes with an emphasis on forest cover change for protected areas and their environs in southern Ghana are mapped and quantified based on Landsat multi-temporal composite data. Second, the magnitude of forest loss in relation to population growth between 2000 and 2010 is examined. Closed forest cover and other land-cover and land-use types are mapped for three

study periods from 1986 to 2018. Changes in forest cover are quantified and examined in conjunction with high spatial resolution satellite images to identify the corresponding causes of land change. A regression analysis is utilized to evaluate the potential anthropogenic pressure on forest cover by examining the statistical relationship between forest loss and population growth.

4.2. Study Area and Data

Figure 7 shows the protected areas and forest reserves in the Western, Ashanti, Eastern, and Central regions of Ghana that are selected for this study. The selected 76 reserves are located in the tropical evergreen forest zone and within a single Landsat image scene. Among the selected reserves is a fully protected reserve, Kakum National Park. Kakum National Park is located in the Central region in Ghana. Established in 1931, Kakum National Park is currently being considered listed as one of the UNESCO World Heritage Sites for its high biodiversity and aesthetic values. Kakum National Park covers a total of 212 km^2. Poaching has been identified as one of the main wildlife threats in this area (Hawthorne & Abu-Juam, 1995). Farming activities surrounding the park are key deforestation drivers. Subri River, the largest reserve in Ghana (588 km^2) is a production reserve in the study area. Other production reserves are included as well, such as Opon Mansi and Bowiye Range. Reserves that are near some of the largest open pit mines in Ghana are also included (e.g., Bonsa Ben, Oda River, Anwhiaso, and Wassaw Conservation Areas). Many potential anthropogenic disturbances exist in these protected areas besides mining, including villages located at the reserve boundaries, large-scale commercial agriculture, and logging exploitation. Based on the average one-way walking time for firewood collection in rural Ghana (Calvo, 1994; United Nations, 2010), a 1.5 km

surrounding area of each reserve is incorporated in addition to the reserve lands as the mapping area for this study, as seen in Figure 7. Based on a polygon shapefile of protected areas provided by the Forestry Commission of Ghana, a subset and buffer of the reserves was created to delineate the mapping area. The total designated reserve area in this study is about 5370 km^2, and the total mapping area (i.e., reserves and environs) is about 9800 km^2.

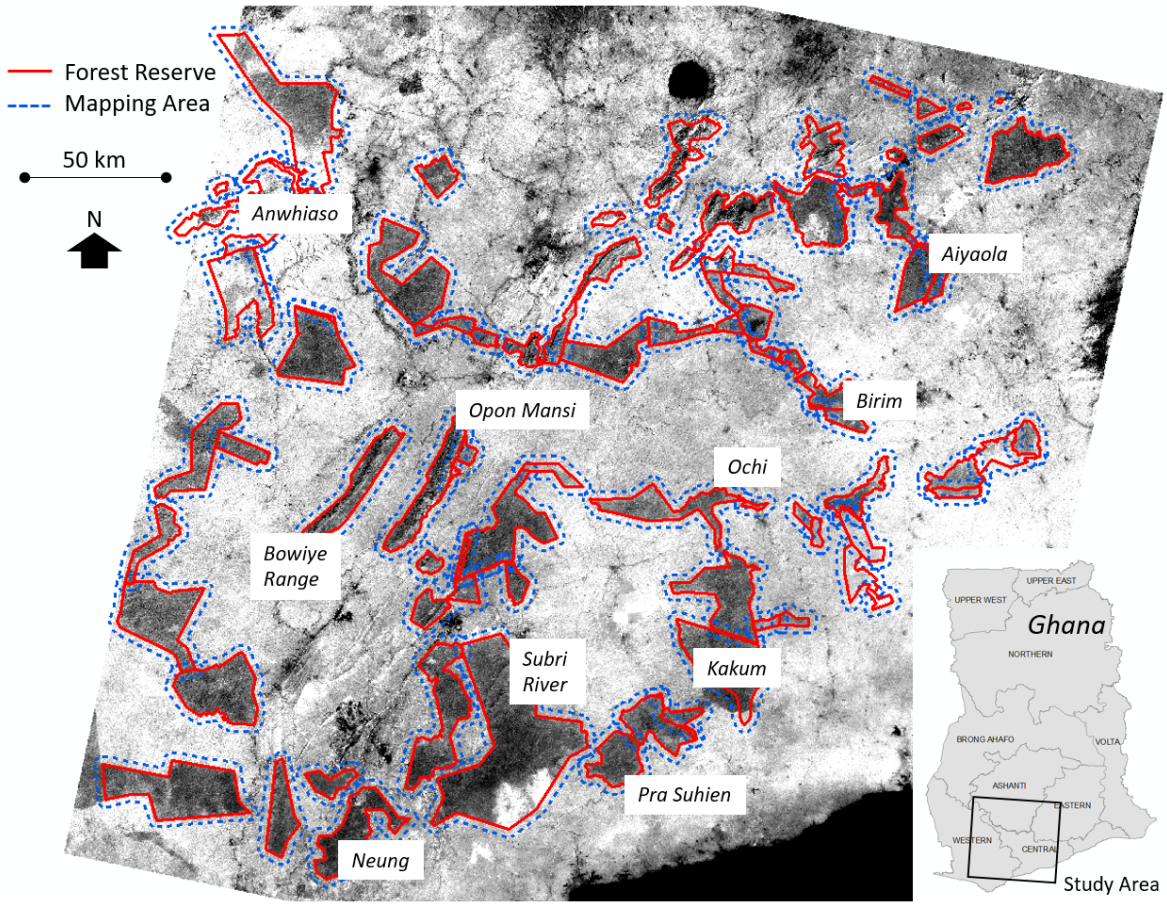

Figure 7. Study area map showing forest reserves (outlined in red) and the mapping area (blue) in southern Ghana. Reserves are located in Western, Central, Eastern, and Ashanti regions. The gray-scale base image is the NIR band of a Landsat 8 OLI image captured in December 2015.

Surface reflectance image products located at Worldwide Reference System 2 path 194 and row 56 collected from Landsat 4 and 5 Thematic Mapper (TM), Landsat 7 Enhanced

Thematic Mapper Plus (ETM+) and Landsat 8 Operational Land Imager (OLI) platforms were reviewed interactively on the Google Earth Engine platform (https://earthengine.google.com) and USGS Earth Explorer (https://earthexplorer.usgs.gov). The imagery data were limited to only Landsat Tier-1 surface reflectance products for they meet certain radiometric and geometric standards during processing to ensure a consistent data quality that supports multi-temporal image analysis (Hall, Strebel, Nickson, & Goetz, 1991; Moran, Jackson, Slater, & Teillet, 1992; USGS https://landsat.usgs.gov/landsat-level-1-standard-data-products). Few Landsat 4 and 5 TM images are available for the study area due to a lack of a data recording station prior to the launch of Landsat 7 in 1999. Landsat 7 images collected after mid-May 2003 were not considered due to the Scan Line Corrector issue for the ETM+ sensor. Based on image and reference data availability, three study periods were selected for this study—circa 1986, circa 2000, and circa 2018. The circa 1986 composite image is composed of six Landsat 4 and 5 TM images collected between 1986 and 1991, including one mostly cloud-free image. The circa 2000 composite image is generated from 39 Landsat 7 ETM+ image scenes captured from January 1999 to mid-May of 2003. The circa 2018 composite image consists of multispectral data from 41 Landsat 8 OLI images collected between 2013 and 2018.

Some high spatial resolution satellite imagery collected in recent years for southern Ghana were available as reference data. QuickBird and IKONOS images were available for viewing on Google Earth. WorldView-2 and a Digital Globe high spatial resolution commercial satellite image mosaic (collected between 2012-2014) is available for viewing as the BaseMap Imagery product in ArcGIS software. Three-meter spatial resolution Planet imagery collected in Fall 2017 and Spring 2018 are also available through the Planet

Education and Research program (Planet Team, 2017). Four relatively cloud-free Landsat images were identified and downloaded from Earth Explorer for visual interpretation. The images corresponding to the study periods were collected in December 1986 (Landsat 5), October 1991 (Landsat 4), May 2002 (Landsat 7), December 2015, and January 2018 (both Landsat 8).

4.3. Methods

Landsat surface reflectance products were retrieved and processed using Google Earth Engine code editor platform. Images were masked for clouds, cloud shadow, and water bodies using the pixel quality assessment band (i.e., pixel_qa) that was derived by the C version of Function of Mask algorithm (CFMask; Foga et al., 2017) and provided as part of the Landsat surface reflectance products. A reflectance normalization process developed by Wu (2004) was applied to the Landsat surface reflectance images to correct for terrain effects. Each spectral band was divided by the sum of all spectral bands for each image date to minimize the illumination differences. The illumination normalized data were used for the subsequent image analysis.

Median value image composites were formed using the available cloud-free pixels for the study periods. Besides the Landsat spectral bands, spectral variability vegetation index (SVVI) and a SVVI texture image were also generated. SVVI was developed through exploratory analysis in a previous study mapping land-cover and land-use in southern Ghana (Coulter et al., 2016). It is calculated as the difference between standard deviation (SD) of all Landsat spectral bands and standard deviation of infrared bands for a given pixel, as defined in Equation 3 of Chapter 2. The SVVI metric was found to effectively minimize

image compositing artifacts and enhance the spectral and textural difference between natural vegetation and subsistence agriculture land in the southern Ghana study area.

SVVI was calculated for each image date captured within the study periods, and composited using the median value for each pixel within the dense time stack. Forest and moist natural vegetation exhibits a low and more homogeneous SVVI value compared to non-vegetated areas. Thus, texture images were generated based on the SVVI products, calculated with a 3-by-3 focal standard deviation function to further differentiate forest and other non-forested land-cover types. A SVVI texture composite image was subsequently created using the median pixel values of the entire time series.

The median value composite layers of red and near infrared spectral bands, SVVI, and SVVI texture were layerstacked and utilized as the land-cover classification input. An unsupervised image classifier using K-means clustering was utilized to classify the images. Five hundred image pixels within the mapping area were randomly selected as the image classifier training data. Spectral clusters were generated by the K-means image classifier while the number of clusters was experimented iteratively. The cluster images were examined in conjunction with high spatial resolution reference imagery and relatively cloud-free single-date Landsat imagery for the corresponding study period. Image clusters were merged and labeled manually into three classes: forest, agriculture/open canopy, and built/bare/surface mining. The forest class represents the undisturbed dense forest, mostly seen as closed canopy forest cover. The agriculture and open canopy class includes sparse secondary forest regeneration, oil palm/cocoa plantations, low-intensity subsistence agriculture, and fallow land. The built, bare, and mining class includes built-up, roads, cleared land with exposed soil, and surface mining. After the image classification, a 3-by-3

focal majority smoothing function was applied to the Landsat-derived maps to yield a more generalized map at a more appropriate minimum mapping unit (closer to 1 ha) and reduce per-pixel classification noise.

Classification accuracies were assessed using a total of 120 reference image pixels. The reference pixels were generated in a random sampling manner, and interpreted in conjunction with available high spatial resolution reference imagery and relatively cloud-free Landsat images to identify the corresponding land-cover and land-use types. Forty samples for the three mapping classes—forest, agriculture/open canopy, and built/mining were created and reviewed to ensure the reference pixels represented stable land-cover and land-use types during c. 1986 to 2018. The resulting reference pixels were used to measure mapping accuracy of each study period. The mapping agreement, user's, producer's, and overall accuracies were summarized in an accuracy assessment table.

Land-cover and land-use change maps were generated based on the multi-temporal Landsat-derived map products through post-classification map comparison. Spatial patterns of forest loss (e.g. locations where closed forest transitioned to non-forest classes) were examined in both quantitative and qualitative manners. Areal data of forest loss was summarized at the reserve and census district levels. Districts are relatively large census units composing multiple enumeration areas (similar to census blocks in the US) and each district encompasses multiple forest reserves. Areal summaries of reserves were aggregated to the district level prior to analysis. Only districts that contain 15% or greater amounts of reserved land were selected for analysis. There are 14 districts within the study area that meet the 15% areal threshold.

Regression analyses were carried out to examine the amount of forest loss in relation to population density and population density change. Forest cover change was summarized for c. 2000-2018. Population data were derived from the decadal Ghana Population and Housing Census (PHC) from years 2000 and 2010. The PHC data are georeferenced to the Enumeration Area (EA) level. Population density of EAs that are within a 1.5 km distance from the reserve boundary was aggregated for each reserve. Population density was also summarized to the census district level, and compared to the forest cover change amounts within each district. Two other independent variables (i.e., cooking fuel types and occupations) were also examined but the data variance was too limited to enable statistical analyses.

4.4. Results

Land-cover and land-use maps for c. 2000 and 2018 are shown in Figure 8. The c. 1986 and 2018 images generated using K-means clustering were based on 25 spectral clusters while the c. 2000 image was created with 16 spectral clusters. Mapping accuracies for the Landsat-derived maps are shown in Table 10. High overall mapping accuracies were achieved for all three study periods, with the overall classification accuracies at 87, 94, and 90% for c. 1986, 2000, and 2018, respectively. As Table 10 shows, some confusion occurred between the forest and open canopy vegetation classes, with slight confusion between built and open canopy vegetation for all three image dates. The forest class appears to be over-classified, particularly for the c. 2000 and 2018 dates, as the user's accuracies are slightly lower than the producer's accuracies. The open canopy/agriculture class on the other hand is under-classified, with higher user's accuracies compared to producer's accuracies. The

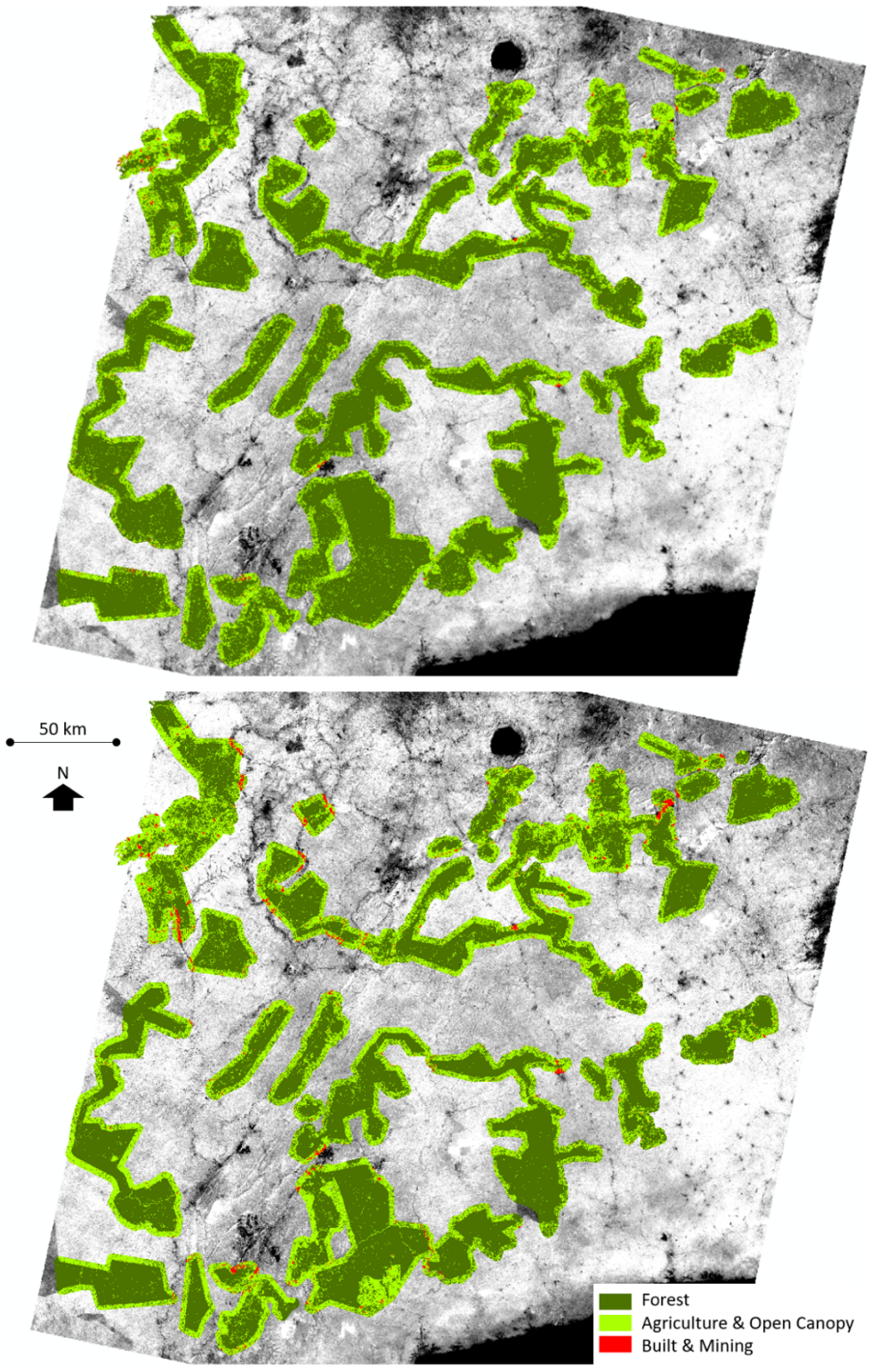

Figure 8. Land-cover and land-use maps for circa 2000 (top) and circa 2018 (bottom). The mapping area includes forest reserves and a 1.5 km outward buffer region from reserve boundaries. The background is a gray-scale NIR Landsat 8 image from December 2015.

built/mining class is mapped with high accuracy, with nearly 100% producer's and user's accuracies for all three dates. The overall forest mapping accuracies of the c. 1986 map are the lowest of all products. The northern portion of the map is particularly problematic, as forest was commonly classified as open canopy/agriculture. This is likely a result of the limited number of images in the composite and lower image quality.

Table 10. Mapping accuracies of the Landsat-derived classification products for circa 1986, 2000, and 2018, respectively. The accuracies were evaluated using 40 reference pixels per class, 120 pixels total for each study period.

Image-derived Class	**Reference Class**									**User's Accuracy %**		
	Forest			Agriculture & Open Canopy			Built & Mining					
	1986	2000	2018	1986	2000	2018	1986	2000	2018	1986	2000	2018
Forest	33	39	37	7	5	8				83	89	82
Open Canopy	7	1	3	33	35	32	2	1	1	79	95	89
Built							38	39	39	100	100	100
Producer's Accuracy %	83	98	93	83	88	80	95	98	98	Overall Accuracy %		
										87	94	90

As seen in Figure 8, the dense evergreen forest cover is generally constrained within reserve boundaries. Open canopy and agriculture are mostly found outside of reserves. Some small patches of forest were mapped beyond reserve boundaries, while mixed in with agriculture and open canopy. Unpaved roads inside reserves, forest clearing and regeneration were also classified as open canopy. Built and surface mining are found near and within reserves. Some changes in forest cover and non-forest vegetation are apparent from the Landsat-derived classification products. About 80 km^2 of forest clearing is identified in Subri River forest reserve in the south of the mapping area between 2000 and 2018. Anwhiaso East reserve located in the northeastern portion of the mapping area, also shows forest loss during this period. Expansion in built and mining land use is also

observed, particularly on the western side of the study area. Roads within reserve lands increased, or at least became more definable in Landsat images captured during the 2000 to 2018 period.

Table 11 summarizes areal land cover and land use and change between the three image periods for the entire mapping area (i.e., almost 9800 km^2), which varies slightly between image dates and data coverage. The percent areal change is calculated as relative change, which is the difference between two mapping dates relative to the earlier date. A total of 6655 km^2, or 68% of the mapping area was mapped as forest cover in c. 2000, the highest of the three study periods. Forest cover increased by 1557 km^2 (a 31% relative increase) from 1986 to 2000, and decreased by -625 km^2, or -9% between c. 2000-2018. Open canopy and agriculture land exhibit the opposite temporal dynamics, with a decrease of over 1500 km^2 in the earlier periods and an increase over 535 km^2 (18% relative increase) since 2000. Built, bare, and surface mining showed a consistent increase in area, with a tripling of area coverage since 1986.

Table 11. Areal summary and change of forest, agriculture/open canopy, and built/bare/mining classes for the entire mapping area in southern Ghana. The areal summary shows the area mapped for each class and the percentage relative to the mapping area. The areal change is calculated as the difference between image dates and percent change compared to the earlier date. Units are in km^2.

Image Date	Mapped Area (km^2)		
	Forest	Agriculture & Open Canopy	Built & Mining
c. 1986	5098 (52%)	4593 (47%)	53 (0.5%)
c. 2000	6655 (68%)	3051 (31%)	70 (0.7%)
c. 2018	6030 (62%)	3586 (37%)	153 (1.6%)
1986-2000 Change	+1557 (31%)	-1542 (-34%)	17 (32%)
2000-2018 Change	-625 (-9%)	535 (18%)	83 (119%)

Figure 9 shows the land-cover and land-use change map between c. 2000 and 2018 for the study area. Most of the reserve land remained dense forest canopy between c. 2000 and

2018, about 5142 km^2 in area. Almost 1500 km^2 of forest in c. 2000 transitioned to open canopy or agriculture land in c. 2018 (shown in blue in Figure 9), mostly found in the western portion of the study area. Over 2000 km^2 of land remained open canopy or agriculture land during this period, most of which are outside the protected area boundaries. Besides road network expansion through forest reserves creating linear patterns of forest loss, logging, mining, and agriculture development contributed to most of the large-scale forest conversion. Over 110 km^2 was mapped as built and mining expansion (from both forest and agriculture/open canopy as seen in pink and green respectively in Figure 9). Large groupings of new built and mining occur northwest, northeast, and south in the portions of

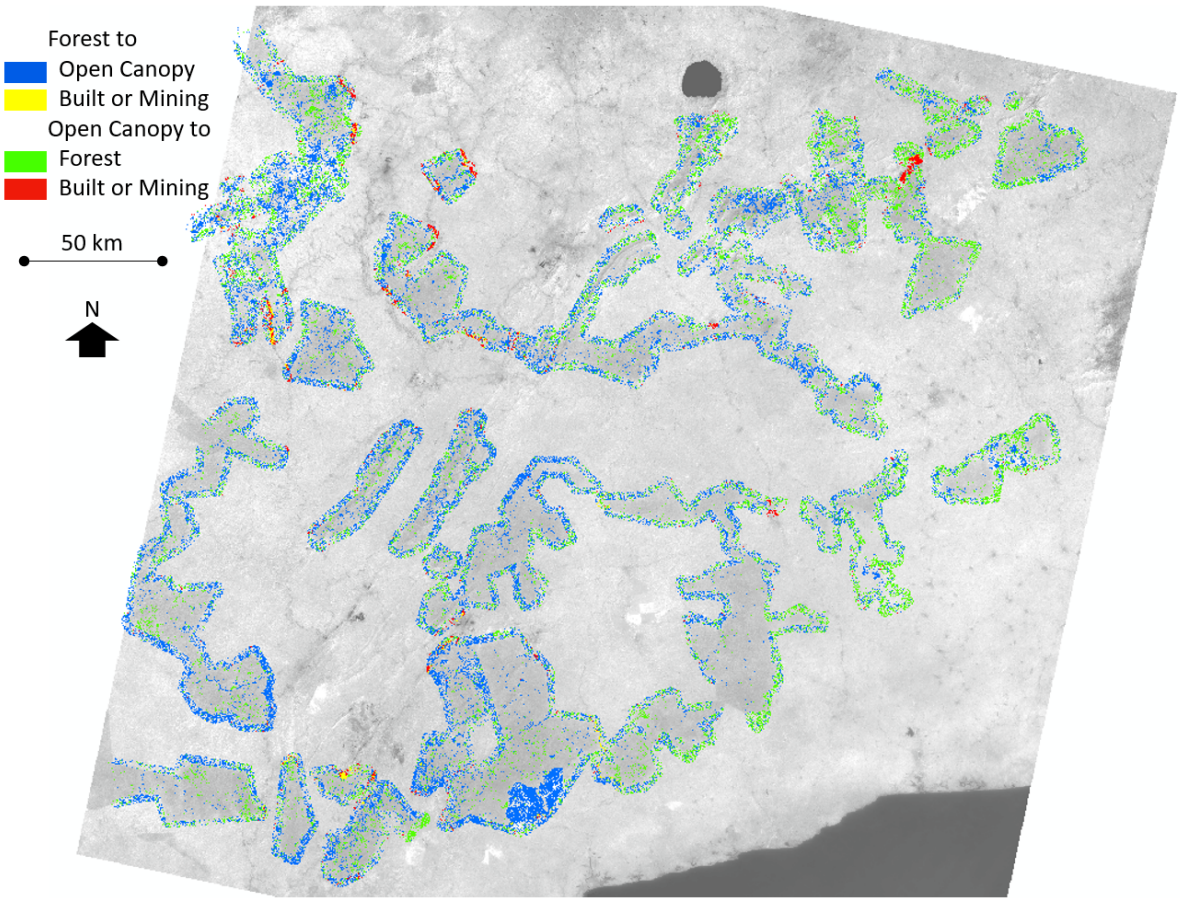

Figure 9. Land-cover and land-use change map of southern Ghana between circa 2000 and 2018. The gray-scale background image is the NIR band of a Landsat 8 December 2015 image.

the mapping area. Mining expansion is observed within reserves northwest of the study area in the c. 2000 to 2018 period.

Forest cover within reserve boundaries is observed to be more fragmented and declined near reserve boundaries in Figures 8 and 9. Forest cover was quantified based on inward buffer zones from reserve boundaries to evaluate edge effects (Murcia, 1995), and an areal summary is shown in Table 12. Forest cover and forest cover change both exhibit substantial fragmentation and reduction near reserve boundaries. Forest cover increases from 88% to 93% in c. 2000 moving from reserve boundaries to the interior of reserves. The proportion of forest for c. 2018 exhibits a similar pattern but lower portion compared to 2000. The 2018 forest cover shows a gradual increase from 82 to 90% as the distance inward from reserve boundaries increases. Areas within 500 m of reserve boundaries show the greatest forest to non-forest transition between c. 2000 and 2018. A 13% relative forest loss from 2000 to 2018 is observed within this 500-m buffer zone from reserve boundaries. Essentially no difference in forest cover or forest loss is observed for the buffers 500-1000, 1000-1500 and 1500-3000 m from reserve boundaries.

Table 12. Areal summary of forest cover in relation to distance from reserve boundary. Forest loss is measured as the area that transitioned from forest in 2000 to non-forest in 2018, with the percentage showing the relative forest loss compared to forest in 2000.

Distance from edge (m)	Total Area (km^2)	2000 Forest (km^2)	2018 Forest (km^2)	Forest Loss (km^2)
0-500	927	818 (88%)	762 (82%)	108 (13%)
500-1000	816	756 (93%)	728 (89%)	65 (9%)
1000-1500	680	634 (93%)	610 (90%)	53 (8%)
1500-3000	1145	1068 (93%)	1030 (90%)	87 (8%)

4.4.1. Reserve Level Analysis of Land-Use and Population Change

Within the designated forest reserve areas, a total of 181 km^2 of forest transitioned to non-forest cover (i.e., open canopy and built) between c. 2000 and 2018. This represents a -

4% decrease relative to the forest area mapped in c. 2000. Most of the reserves have a slight forest cover decrease during this period. Three reserves show over -25% relative forest loss in c. 2018 when compared to the c. 2000 forest area, namely Anhwiaso North, Anhwiaso East, and Afoa Hills. These three reserves are located at the northwest end of the study area, and have large-scale open pit mines nearby. Open pit mines are mapped within Afao Hills for all three study periods, with mining expansion during c. 2000-2018. A few reserves in the northeast of the mapping area show slight forest increase between c. 2000 and 2018. These include Aiyaola, Nsuensa, Bediako, and Mamang River Reserves. Despite being near mining activity, these reserves are also near large-scale plantation and commercial agriculture lands. When including the 1.5 km buffer region as reserve environs, eight reserves (including the three mentioned previously) have over -25% forest loss in c. 2018 compared to the forest area in c. 2000. All but one reserve is located in the western portion of the study area, and adjacent to mines. Kakum National Park shows a 0.6% increase in forest cover by c. 2018 compared to the c. 2000 forest area within the park boundary. The park and its environs combined exhibit a 2.98 km^2 increase in forest area, or 1.3% during c. 2000-2018. Subri River, where large-scale forest clearing was observed from the classification maps, reflects a -11% relative forest decrease within the protected area during c. 2000-2018. This is likely due to forest plantation activity between planting and clear-cutting, as observed on the high spatial resolution reference images.

Figure 10 shows scatterplots between population density change and forest cover change. The estimated population derived from the 2000 and 2010 census showed an increase in population for all the reserves (aggregated from EAs) and districts within the mapping area. As Figure 10a shows, no significant correlation (R^2 of 0.05; p=0.1770) was found between population density change and forest cover loss at the reserve level. Due to the limited available EA boundary coverage, only the northern and eastern parts of the study area (a total of 38 reserves) were analyzed for the relationship between forest cover change and population gain. All the analyzed reserves show population increase and forest loss with varying degree. Annual population density change between 2000 and 2010 ranged from an increase of 1 to 14 people km^{-2} yr^{-1}, with an average of 2 people km^{-2} yr^{-1} (rural Ghana average population increase is about 1 person km^{-2} yr^{-1}). The average relative forest cover loss between c. 2000 and 2018 per year is -1.3% and ranged from -0.4 to -2.3%. Ochi Headwaters forest reserve had the greatest increase in population density among the analyzed reserves, and also had a high relative forest loss at -37%. The Landsat-derived

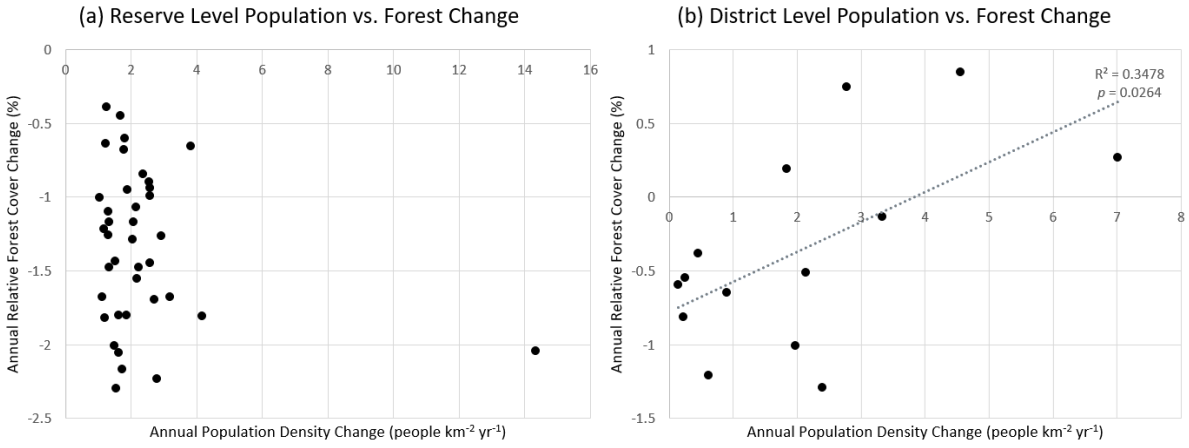

Figure 10. Scatterplots of regression models for annual population density vs. forest cover change at the reserve level (a) and census district level (b). Annual population density was derived from the 2000 and 2010 censuses, and the annual relative forest cover change was measured based on the c. 2000 and 2018 Landsat-derived classification maps.

land-cover and land-use maps also indicated large-scale built expansion (from the town of Asin Foso) adjacent to both north and south ends of Ochi Headwaters. The reserve was established to protect the Ochi River water source (Hawthorne & Abu-Juam, 1995). Despite this goal, the Landsat-derived maps indicated drastic forest reduction from agriculture activity in the reserve. Anwiaso East reserve exhibited the greatest relative forest cover loss, with average population density increase of 2 people km^{-2} yr^{-1} (or 6% annual increase) between 2000 and 2010. Kakum National Park area had a low population density increase at 1 person km^{-2} yr^{-1} (12% annual increase).

4.4.2. District Level Analysis of Land-Use and Population Change

Table 13 shows the forest area mapped for c. 2000 and 2018 aggregated to the census district level, along with the population density for 2000 and 2010. Four out of the 14 districts showed forest cover increase, namely Ashanti Akim, Asikuma, Birim North, and Birim South. Birim North had the most forest increase of 29 km^2 or 15% compared to the forested area in 2000. These four districts are located on the eastern side of the mapping area, as a vertical contiguous region. The remaining ten districts showed forest cover decrease, ranging from -13 km^2 (Assin district) to -165 km^2 (Wassa Amenefi). Percentage wise when comparing to the c. 2000 forest area, forest loss ranges from -3 (Assin) to -23% (Bibiani). Wassa Amenefi and Bibiani districts are adjacent to each other, located on the western edge of the study area. Assin district, where Kakum National Park is located, showed the least forest loss between 2000 and 2018.

At the district level, population density change between years 2000 and 2010 shows a modest (R^2 of 0.35; $p = 0.0264$) inverse relationship with the amount of forest change between c. 2000-2018, as seen in Figure 10b. On average, a 2 people km^{-2} yr^{-1} increase was

observed at the district level. In districts where there was forest reduction, population density showed mild increase, ranging from a gain of 1 to 3 people km^{-2} yr^{-1}. In districts where forest cover was mapped as increase between c. 2000-2018, population density also showed greater increase. In the Bibiani district where forest cover reduced the most, annual population density change was average, at a 2 people km^{-2} yr^{-1} increase. No correlation (R^2 = 0.008; p = 0.8006) was found between annual population density change and the amount of forest cover loss when excluding the four districts of forest cover increase.

Table 13. Mapped forest areal summary of 14 census districts for c. 2000 and 2018, and population density for 2000 and 2010 derived from census data. The areal change is calculated as the difference between image dates and percent change compared to the earlier date. Units are in km^2. Population density is measured as the number of people per km^2 for a given district.

District	Forest Area (km^2)			Population Density (people km^{-2})		
	2000	**2018**	**Change**	**2000**	**2010**	**Change**
Birim N.	189	218	+29 (15%)	107	152	45 (42%)
Asikuma	132	149	+17 (13%)	118	146	28 (24%)
Birim S.	306	320	+14 (5%)	143	213	70 (49%)
Ashanti Akim S.	183	189	+5 (3%)	83	101	18 (22%)
Assin	507	494	-13 (-3%)	93	126	33 (35%)
Twifu	386	359	-27 (-7%)	72	77	5 (7%)
Amansie E.	369	335	-34 (-9%)	113	134	21 (19%)
Nzema E.	366	330	-36 (-10%)	69	71	2 (3%)
Mpohor Wassa	869	776	-93 (-11%)	57	58	1 (2%)
Obuasi	608	537	-71 (-12%)	157	166	9 (6%)
Wassa Amenefi	1129	964	-165 (-15%)	49	51	2 (4%)
Amansie W.	211	173	-38 (-18%)	91	111	20 (22%)
Wassa W.	631	494	-137 (-22%)	86	92	6 (7%)
Bibiani	228	175	-53 (-23%)	124	148	24 (19%)

4.5. Discussion and Conclusions

Land-use dynamics of over 70 forest reserves of tropical forest and the reserve environs were examined in this study. Dense Landsat image time series and median value SVVI composites were found effective in minimizing affects of no-data pixels due to cloud cover, and yielded high classification accuracy in the cloud-prone southern Ghana area. The median value SVVI composites used in this study show no residual clouds or other

compositing artifacts, an improvement compared to the maximum value composites used previously by Coulter et al. (2016). The c. 1986 product exhibits lower mapping accuracy, most likely due to lower Landsat image quality, more limited and uncertain reference data, and because few images are available to generate multi-temporal composite images. Some mapping confusion is apparent, as open canopy was mapped as closed forest for all three image dates. Most misclassified pixels are associated with areas located outside of reserve boundaries, where secondary regeneration, plantation, and off-reserve forest could be confused with dense on-reserve forest cover. Available high spatial resolution imagery is limited for c. 1986 and c. 2000, creating a challenge for generating reliable reference data for accuracy assessment. This could also lead to mapping disagreement and uncertainty, particularly between open canopy and forest classes.

Land-cover and land-use change is most commonly associated with anthropogenic processes (IGBP report, 1993; UNEP GEO-5 report, 2012). In this study, anthropogenic activities such as mining, plantation/logging, agriculture and built expansion are observed in southern Ghana from 1986 to 2018, resulting in declining forest cover and secondary regeneration/open canopy, even within protected areas. While subsistence farming and built expansion are the common and wide-spread threats to forest loss, other factors are more localized. Large-scale open pit mines expanded in a concentrated manner in the northwestern side of the study area (e.g., Anwhiaso) during 2000-2018. Although few mines are present within protected areas, drastic forest reduction is observed at both the reserve level and district level. While mining was also observed near reserves in the northeast of the study area, large-scale commercial agriculture/plantation is also present. Hawthorne and Abu-Juam (1995) documented logging activity and open canopy within these reserves, but

observed concomitant forest regeneration. This may explain why extensive forest cover loss was not observed in the northeast region. Large-scale plantation activities such as afforestation and forest clearing are observed in reserves within the southern part of the study region (e.g., Subri and Neung) as another source of land change. The commonly practiced taungya systems might increase human disturbances through additional subsistence agriculture activity within plantations in Ghana, leading to forest cover change.

The livelihoods of rural households in Ghana heavily depend on forest-related income (Appiah et al., 2009; FAO, 2016). While a growing rural population could mean increasing reliance on forest resources, no correlation was found between the magnitude of forest and population change at the reserve level and a weak significant positive correlation at the district level in this study. The population density increase in the study area is relatively low with little variance, particularly at the reserve level (2 people km^{-2} yr^{-1}). At the district level, the population data are summarized from a larger spatial extent (i.e., including areas located far from forest reserves) than the mapped forest cover. Although percentage and density were used to standardize areal estimates, differences in area between census and land use analytical units likely influence uncertainty in the regression analysis. More forest conservation efforts could also arise from scarce forest resources due to population increase (López-Carr & Burgdorfer, 2013), resulting in less forest loss or even forest recovery. Deforestation has been associated with population growth in varying ways in other studies. Mertens and Lambin (2000) examined deforestation in South Cameroon with various potential land-cover and land-use change causes. They found that at the village level, deforestation is positively related to population growth while the highest magnitude of deforestation was found in villages with small population. On the other hand, population

density has been found to have insignificant relationship with deforestation rate in the Brazilian Amazon (IGBP report, 1993). DeFries, Rudel, Uriarte, and Hansen (2010) also found that tropical forest loss is not associated with rural population growth at a global scale. These varying results suggest that deforestation can be a complex type of land-cover and land-use change, and population alone might not be a sufficient predictor of forest loss (Lambin et al., 2001). Other factors such as affluence, land management policies, macro-economic, and political influences should also be considered in future studies.

Different types and magnitudes of land-cover and land-use changes were observed between protected and production reserves in this study. Kakum National Park, a protected reserve, exhibited minimal land-cover and land-use change, and relatively stable forest cover during the study periods. In addition to Kakum National Park, a cluster of reserves included in the Greater Kakum working plans (including Assin and Pra Suhien) all showed stable forest cover between c. 2000 and 2018. Production reserves such as Subri River, Bowiye Range, and Opon Mansi each have a substantial plantation/productive area. These reserves all had over -16% relative forest loss during 2000-2018 as mapped in the classification products. The variation suggests that reserve regulations and policies could be an influential factor in forest protection. Land management of protected areas is often defined locally in Ghana, because of the mostly private land ownership. Reserve management goals can vary from protection of forests from logging and development, to protecting particular tree species, to protecting game and wildlife. Due to the variations in land ownership and management goals, a local or regional scale, such as the reserve and district levels used in this study, is appropriate for analyzing patterns of forest loss.

The data utilized in this study presented a few challenges. The limited availability of high spatial resolution imagery as reference data led to higher uncertainty for accuracy assessment of land-cover and land-use change products. The mapped land-use changes were particularly difficult to verify, especially for earlier study periods of c. 1986 and 2000. Few Landsat 4 and 5 TM images were available for the early part of the study period, reducing the quality of the multi-temporal image composites. For the census data, EA boundaries were generated so that each delineated area contains similar populations. Following population increase, the EA boundaries were modified by Ghana Statistical Services between 2000 and 2010 census. Fortunately, because of the mostly rural mapping area, the discrepancies between the years were relatively minor. EA boundaries were ensured to share similar spatial extents. Because EA boundary files for 2010 are not completed for all of Ghana, the analysis of population and forest change relationship was limited to the eastern portion of the study area, where the boundary files had been completed.

Google Earth Engine is open-access for education, research, and non-profit users. It provides an image library and a JavaScript coding platform for geospatial data analysis. Users can interactively implement and execute processes, and view results in an efficient manner utilizing its powerful cloud-based computing resources. The platform enabled dense time series of Landsat images to be processed, images to be composited, and unsupervised classification to be efficiently and effectively performed for this study, in just a few minutes. The image library eliminated the need for downloading a large quantity of imagery data. Compared to conventional image processing software, no license or installation is required for Earth Engine. Earth Engine platform could provide valuable resources for land-use and land-cover monitoring in a timely manner.

Monitoring forest resources for conservation and ecological purposes is critical, especially with the rapid population and economic growth of sub-Saharan Africa and Ghana. The mapping approach implemented on the cloud-based Google Earth Engine using median value SVVI composite images was effective and efficient for monitoring forest cover and other land-use changes in the extremely cloud-prone southern Ghana. Other forested and cloud-prone regions could also benefit from this mapping approach. Future research should focus on exploring other anthropogenic factors that are potentially associated with deforestation to target management efforts. More frequent and extensive land-use monitoring could provide valuable information for government agencies to regulate and enforce logging and mining permits. Improved and updated land change estimates, as demonstrated with the mapping methods in this study, could also be used to support conservation efforts.

Chapter 5. Conclusions

5.1. Summary of Results

The goals of this research were to (1) develop and test novel approaches to map forest cover and monitor its change, and (2) examine human influences on land-cover and land-use changes in forest reserves and their environs. The goals were achieved by developing reliable image processing workflows for satellite image-based vegetation and land-use change mapping, and examining anthropogenic causes of land change for protected areas in China and Ghana. These image processing workflows were implemented on the open-access, web-based geospatial analysis platform Google Earth Engine to increase the utility of the mapping approach.

The study presented in Chapter 2 evaluated different advanced image classification techniques for mapping complex vegetation compositions and land-use types in the cloud-prone and extremely mountainous Fanjingshan National Nature Reserve (FNNR) in China. Mixed evergreen and deciduous vegetation types were found to be the dominant forest cover types in the reserve based on the Landsat-derived classification products. Evergreen broadleaf type shows a distinct distribution along river and stream channels. Deciduous cover is concentrated on the high elevation ridges and the southern end of the reserve. The eastern side of the reserve has more bamboo cover, while the western side has more conifer. A combination of image processing techniques was concluded to yield reliable and consistent forest and land-use maps with moderate, above 70% mapping accuracies. Multi-seasonal Landsat image composites minimized the persistent cloud cover issue. Elevation ancillary data, spectral vegetation index products, and shade/illumination normalization approaches suppressed terrain effects and improved mapping accuracy. Important image

classifier parameters were tuned using cross-validation and grid search techniques for optimizing the performance and accuracy of a random forest machine learning image classifier.

The utility of monitoring land-use dynamics using the mapping workflow developed in Chapter 2 was assessed in Chapter 3, through mapping and quantified vegetation and land-use transitions in FNNR over a 28-year period, including afforestation related to payment for ecosystem services programs and anthropogenic development. Land-use transitions were reliably identified by implementing logical land-use transition rules with map pixels that changed from-to classes of interest. Approximately 10-12 km^2 of land area was mapped as afforestation, mostly in the reserve environs along roads and river channels. Despite the protected status, anthropogenic activities within and adjacent to the reserve boundary are prevalent. A substantial amount of development was observed in the reserve environs, and the reserve core area also experienced sporadic land-use changes. Built development mainly corresponds to the expansion of roads and freeways, and construction of tourism and recreational infrastructure.

In Chapter 4, forest and land-use types were mapped and changes were assessed for multiple reserves in southern Ghana over a 30-year period, utilizing dense Landsat images and the median value spectral vegetation variability index (SVVI) composites. The magnitude of forest loss in relation to population growth was also examined. The Landsat-derived forest and land-use maps yielded high classification accuracies, ranging from 87 to 94%. Dense evergreen forest was found mostly constrained within reserve boundaries. Most reserves exhibited forest loss during the mapping period, mostly due to mining, agriculture, and built expansion. Extensive mining expansion was observed in the western side of the

study area and likely led to substantial amounts of forest loss in the surrounding region. Large-scale plantations and their associated forest cover change were also observed.

Collectively, this research provides a remotely sensed image processing workflow that can be utilized for land-cover and land-use change monitoring in cloud prevalent and mountainous areas, and an effective approach for long-term environmental monitoring. Land-use dynamics and the associated anthropogenic activities were also documented for selected forest reserves in two developing countries, China and Ghana. Such workflow implemented on open-access and cloud-based geospatial analysis platform Earth Engine increases the image processing efficiency and method accessibility.

5.2. Key Contributions and Findings

This dissertation study contributes to the land-cover and land-use mapping literature by developing and demonstrating utility of optical remotely sensed imagery and multi-temporal image analysis procedures for cloud-prone and mountainous regions. The mapping and monitoring products stemming from these novel approaches provide extensive land-use dynamic information for the study of forest reserves in two developing countries, which may be useful to their reserve managers. Dense time series and median value image composites minimized the cloud cover issue, while illumination normalization approaches suppressed terrain effects. Logical land transition rules during post-classification map comparison ensured that map classes of interest were preserved. Improved and updated land change estimates, as demonstrated in this study, can better inform conservation policy and support land change monitoring for other forested, cloud-prone, and mountainous regions.

Both study areas in this research are in rural regions in developing countries, yet anthropogenic activities were found to be closely associated with land-use transitions within

and near protected areas. Built expansion and infrastructure construction were identified in both study areas. The afforestation effort through the payment for ecosystem services programs was observed in China, while surface mining and plantation were among the dominant land-change types in Ghana.

Efficient image processing capabilities were enabled by the cloud-based Earth Engine platform, from accessing pre-processed Landsat imagery, implementing both machine learning type and unsupervised clustering image classifications, generating map products, to evaluating mapping accuracy. Machine learning type image classifier was utilized when training data were available and yielded reasonable accuracy mapping complex vegetation composition. Unsupervised clustering algorithms were applied to a larger mapping area when training data were not readily available, and yielded highly accurate maps.

Reserve management policies and protection status seems to be an important factor in forest cover change. Sporadic and planned land transitions occurred in China where the central government has significant importance in land management and planning. Conversely, most lands are privately owned and managed regionally by tribes and chiefs in Ghana. It was observed that a fully protected national park in Ghana showed relatively stable forest cover, while other production reserves indicated varying degrees of forest cover loss.

5.3. Future Research

Several aspects of this research should be expanded and further explored. For example, the resultant land-transition maps and their applicability should be further examined. Ecological and conservation studies could benefit from the spatial distribution information provided by the land transition maps. The maps could serve as the basis or be used in

conjunction with other survey data in evaluating ecological and conservation impacts of land change. The efficacy of the afforestation effort and the goals of payment for ecosystem services programs in China could be analyzed, in terms of soil erosion, forest coverage, and slope land stability.

For land-cover and land-use mapping, the developed mapping workflow could be shared and applied to other regions, while its usability and applicability on Earth Engine can be improved. Mapping and monitoring forest and land-use changes with similar approaches could provide more comparable land change information on regional and even global scale. Reserve managers could benefit from the extensive reserve land-cover and land-use monitoring of the cloud-based mapping approach. A web application with graphical user interface that integrates the scripts for the developed method can further minimize the requirement for user training and the coding ability requirement.

In terms of forest cover change in protected areas, factors other than population growth should be explored in order to target management efforts. Reserve management policies and regulation implementation could be surveyed and analyzed with the amount of forest cover loss. The funding and resources that reserves receive might indicate how well the reserves are protected. The knowledge and perception of local residents on forest resources could also shed light on human usage.

References

Aitken, S., An, L., Yang, S., accepted. Development and sustainable ethics in Fanjingshan National Nature Reserve, China. Ann Am Assoc Geogr.

Appiah, M., Blay, D., Damnyag, L., Dwomoh F.K., Pappinen, A., Luukkanen, O., 2009. Dependence on forest resources and tropical deforestation in Ghana. Environ Dev Sustainability 11. 417-487.

Barraclough, S.L., Ghimire, K.B., 2000. Agricultural expansion and tropical deforestation: Poverty, international trade, and land use. London: Earthscan.

Belgiu, M., Drăguţ, L., 2016. Random forest in remote sensing: A review of applications and future directions. ISPRS J Photogramm Remote Sens 114, 24-31.

Bishop, C.M., 2006. Pattern recognition and machine learning. Springer: New York, US.

Bennett, M.T., 2008. China's sloping land conversion program: institutional innovation or business as usual? Ecol Econ 65, 699–711.

Boser, B.E., Guyon, I., Vapnik, V., 1992. A training algorithm for optimal margin classifiers. Proceedings of the Fifth Annual Workshop on Computational Learning Theory, 144–152. ACM Press.

Breiman, L., 2001. Random forests. Mach Learn 45, 5-32.

Breiman, L., Friedman, J., Stone, C.J., Olshen, R.A., 1984. Classification and regression trees. Routledge: New York, US.

Broich, M., Hansen, M.C., Potapov, P., Adusei, B., Lindquist, E., Stehman, S.V., 2011. Time-series analysis of multi-resolution optical imagery for quantifying forest cover loss in Sumatra and Kalimantan, Indonesia. Int J Appl Earth Obs Geoinf 13(2), 277-291.

California Native Plant Society (CNPS) Vegetation Committee Rapid Assessment (RA) Protocol. URL http://www.cnps.org/cnps/vegetation/pdf/protocol-combined-2016.pdf (accessed on November 2017).

Calvo, C.M., 1994. Case study on the role of women in rural transport: access of women to domestic facilities. Washington, DC: World Bank.

Carlson, T.N., Ripley, D.A., 1997. On the relation between NDVI, fractional vegetation cover, and leaf area index. Remote Sens Environ 62, 241-252.

Carr, D.L., 2004. Proximate population factors and deforestation in tropical agricultural frontiers. Popul Environ 25(6), 585-612.

Carr, D.L., Suter, L., Barbieri, A., 2005. Population dynamics and tropical deforestation: state of the debate and conceptual challenges. Popul Environ 27(1), 89-113.

Chen, H.L., Lewison, R., An, L., Tsai, Y.H., Stow, D.A., Shi, L., Yang, S., in review. Assessing the effects of payment for ecosystem services programs on forest structure and species biodiversity. J Appl Ecol.

Chen, H., Marter-Kenyon, J., López-Carr, D., Liang, X.Y., 2015. Land cover and landscape changes in Shaanxi Province during China's Grain for Green Program (2000–2010). Environ Monit Assess 187(10), 644.

Cheong, S.M., Brown, D.G., Kok, K., Lopez-Carr, D., 2012. Mixed methods in land change research: towards integration. Trans Inst of Br Geogr 37(1), 8-12.

Coppin, P.R., Bauer, M.E., 1995. The potential contribution of pixel-based canopy change information to stand-based forest management in the northern U.S. J Environ Manage 44, 69-82.
Coulter, L.L., Stow, D.A., Tsai, Y.H., Ibanez, N., Shih, H.C., Kerr, A., Bensa, M., Weeks, J.R., Mensah, F., 2016. Classification and assessment of land cover and land use change in southern Ghana using dense stacks of Landsat 7 ETM+ imagery. Remote Sens Environ 184, 396-409.
Daily, G.C., Matson, P.A., 2008. Ecosystem services: from theory to implementation. Proceedings of the National Academy of Sciences of the United States of America (PNAS), Proc Natl Acad Sci 105 (28), 9455–9456.
Davies, K.P., Murphy, R.J., Bruce, E., 2016. Detecting historical changes to vegetation in a Cambodian protected area using the Landsat TM and ETM+ sensors. Remote Sens Environ 187, 332-344.
Debinski, D.M., Kindscher, K., Jakubauskas, M.E., 1999. A remote sensing and GIS-based model of habitats and biodiversity in the Greater Yellowstone ecosystem. Int J Remote Sens 20, 3281–91.
DeFries, R.S., Rudel, T., Uriarte, M., Hansen, M., 2010. Deforestation driven by urban population growth and agricultural trade in the twenty-first century. Nat Geosci 3(3), 178.
Dickson, K.B., Benneh, G., Essah, R.R., 1988. A new geography of Ghana. Longman Publishing Group.
Domaç, A., Süzen, M.L., 2006. Integration of environmental variables with satellite images in regional scale vegetation classification. Int. J Remote Sens 27, 1329-1350.
Dorren L.K., Maier B., Seijmonsbergen A.C., 2003. Improved Landsat-based forest mapping in steep mountainous terrain using object-based classification. For Ecol Manage 183, 31-46.
Farr, T.G., Rosen, P.A., Caro, E., Crippen, R., Duren, R., Hensley, S., Kobrick, M., Paller, M., Rodriguez, E., Roth, L., Seal, D., 2007. The shuttle radar topography mission. Rev Geophys 45(2).
Feng, Z., Yang, Y., Zhang, Y., Zhang, P., Li, Y., 2005. Grain-for-green policy and its impacts on grain supply in West China. Land Use Policy 22, 301-312.
Foga, S., Scaramuzza, P.L., Guo, S., Zhu, Z., Dilley, R.D., Beckmann, T., Schmidt, G.L., Dwyer, J.L., Hughes, M.J., Laue, B., 2017. Cloud detection algorithm comparison and validation for operational Landsat data products. Remote Sens Environ 194, 379-390.
Food and Agriculture Organization (FAO) of the United Nations, 2010. Global forest resource assessment, Main report. FAO Forestry Paper 163.
Food and Agriculture Organization (FAO) of the United Nations, 2016. State of the world's forest 2016. FAO, Rome.
Franco-Lopez, H., Ek, A.R., Bauer, M.E., 2001. Estimation and mapping of forest stand density, volume, and cover type using the k-nearest neighbors method. Remote Sens Environ 77, 251-274.
Franklin, S.E., Wulder, M.A., 2002. Remote sensing methods in medium spatial resolution satellite data land cover classification of large areas. Prog Phys Geogr 26(2), 173-205.

Ghana Statistical Service, 2012. 2010 population & housing census summary report of final results. Ghana Statistical Service, Accra.
Global Environmental Facility (GEF) Project Team, 2004. The management plan of Guizhou Fanjingshan National Nature Reserve. Jiangkou: FNNR GEF Project Management Plan Group.
Gorelick, N., Hancher, M., Dixon, M., Ilyushchenko, S., Thau, D., Moore, R., 2017. Google Earth Engine: Planetary-scale geospatial analysis for everyone. Remote Sens Environ 202, 18-27.
Gray, J., Song, C., 2013. Consistent classification of image time series with automatic adaptive signature generalization. Remote Sens Environ 134, 333-341.
Hall, F., Strebel, D., Nickeson, J., Goetz, S., 1991. Radiometric rectification: toward a common radiometric response among multidate, multisensor images. Remote Sens Environ 35, 11-27.
Hall, J.B., Swaine, M.D., 1976. Classification and ecology of closed-canopy forest in Ghana. J Ecol 64(3), 913-951.
Hansen, M.C., DeFries, R.S., Townshend, J.R.G., Carroll, M., Dimiceli, C., Sohlberg, R.A., 2003. Global percent tree cover at a spatial resolution of 500 meters: First results of the MODIS vegetation continuous fields algorithm. Earth Interact 7(10), 1-15.
Hansen, M.C., Potapov, P.V., Moore, R., Hancher, M., Turubanova, S., Tyukavina, A., Thau, D., Stehman, S.V., Goetz, S. J, Loveland, T.R., Kommareddy, A., 2013. High-resolution global maps of 21st-century forest cover change. Science 342, 850-853.
Hansen, M.C., Roy, D.P., Lindquist, E., Adusei, B., Justice, C.O., Altstatt, A., 2008. A method for integrating MODIS and Landsat data for systematic monitoring of forest cover and change in the Congo Basin. Remote Sens Environ 112(5), 2495-2513.
Harkness, J., 1998. Recent trends in forestry and conservation of biodiversity in China. The China Quarterly 156, 911-934.
Hawthorne, W.D., Abu-Juam, M., 1995. Forest protection in Ghana. IUCN, Gland, Switzerland and Cambridge, UK.
Hens, L., Boon, E.K., 1999. Institutional, legal, and economic instruments in Ghana's environmental policy. Environ Manage 24(3), 337-351.
Hilson, G., Nyame, F., 2006. Gold mining in Ghana's forest reserves: a report on the current debate. Area 38(2), 175-185.
Hough, J.L., 1988. Obstacles to effective management of conflicts between national parks and surrounding human communities in developing countries. Environ Conserv 15(2), 129-136.
Huang, C., Goward, S.N., Masek, J.G., Gao, F., Vermote, E.F., Thomas, N., Schleeweis, K., Kennedy, R.E., Zhu, Z., Eidenshink, J.C., Townshend, J.R., 2009. Development of time series stacks of Landsat images for reconstructing forest disturbance history. Int. J Digit Earth 2(3), 195-218.
International Geosphere-Biosphere Programme (IGBP), 1993. Relating Land Use and Global Land-Cover Change: A proposal for an IGBP-HDP core project. Stockholm.
Jensen, J.R., 1996. Introductory Digital Image Processing: A Remote Sensing Perspective, Prentice-Hall, Saddle River, New Jersey.

Johansen, K, Phinn, S., Taylor, M., 2015. Mapping woody vegetation clearing in Queensland, Australia from Landsat imagery using the Google Earth Engine. Remote Sens Appl: Soc Environ 1, 36-49.
Kalame, F.B., Aidoo, R., Nkem, J., Ajayie, O.C., Kanninen, M., Luukkanen, O., Idinoba, M., 2011. Modified taungya system in Ghana: a win–win practice for forestry and adaptation to climate change?. Environ Sci Policy 14(5), 519-530.
Kotsiantis, S.B., Zaharakis, I., Pintelas, P., 2007. Supervised machine learning: A review of classification techniques. Emerging Artificial Intelligence Applications in Computer Engineering 160, 3-24.
Kusimi, J.M., 2008. Assessing land use and land cover change in the Wassa West District of Ghana using remote sensing. GeoJournal 71(4), 249-259.
Lambin, E.F., Turner, B.L., Geist, H.J., Agbola, S.B., Angelsen, A., Bruce, J.W., Coomes, O.T., Dirzo, R., Fischer, G., Folke, C., George, P., 2001. The causes of land-use and land-cover change: moving beyond the myths. Glob Environ Chang 11(4), 261-269.
Lindquist, E.J., Hansen, M.C., Roy, D.P., Justice, C.O., 2008. The suitability of decadal image data sets for mapping tropical forest cover change in the Democratic Republic of Congo: implications for the global land survey. Int. J Remote Sens 29(24), 7269-7275.
Liu, J., Diamond, J., 2005. China's environment in a globalizing world. Nature 435, 1179-1186.
Liu, J., Li, S., Ouyang, Z., Tam, C., Chen, X., 2008. Ecological and socioeconomic effects of China's policies for ecosystem services. Proc Natl Acad Sci 105, 9477-9482.
Liu, J., Linderman, M., Ouyang, Z., An, L., Yang, J., Zhang, H., 2001. Ecological degradation in protected areas: the case of Wolong Nature Reserve for giant pandas. Science 292, 98-101.
Liu, J., Yang, W., 2013. Integrated assessments of payments for ecosystem services programs. Proc Natl Acad Sci 110, 16297–16298.
Liu, L., Tang, H., Caccetta, P., Lehmann, E.A., Hu, Y., Wu, X., 2013. Mapping afforestation and deforestation from 1974 to 2012 using Landsat time-series stacks in Yulin District, a key region of the Three-North Shelter region, China. Environ Monit Assess 185(12), 9949-9965.
López-Carr, D., Burgdorfer, J., 2013. Deforestation drivers: population, migration, and tropical land use. Environ: Sci Policy for Sustainable Dev 55(1), 3-11.
Lu, D., Weng, Q., 2007. A survey of image classification methods and techniques for improving classification performance. Int J Remote Sens 28, 823-870.
Margules, C.R., Pressey, R.L., 2000. Systematic conservation planning. Nature 405, 243-253.
Masek, J.G., Vermote, E.F., Saleous, N.E., Wolfe, R., Hall, F.G., Huemmrich, K.F., Gao, F., Kutler, J., Lim, T.K., 2006. A Landsat surface reflectance dataset for North America, 1990-2000. IEEE Geosci. Remote Sens Lett 3, 68-72.
Masozera, M.K., Alavalapati, J.R.R., Jacobson, S.K., Shrestha, R.K., 2006. Assessing the suitability of community-based management for the Nyungwe Forest Reserve, Rwanda. For Policy Econ 8(2), 206-216.

Matsushita, B., Yang, W., Chen, J., Onda, Y., Qiu, G., 2007. Sensitivity of the enhanced vegetation index (EVI) and normalized difference vegetation index (NDVI) to topographic effects: a case study in high-density cypress forest. Sensors 7, 2636-2651.
Mertens, B., Lambin, E.F., 2000. Land-cover-change trajectories in southern Cameroon. Ann Am Assoc Geogr 90(3), 467-494.
Moran, M.S., Jackson, R.D., Slater, P.N., Teillet, P.M., 1992. Evaluation of simplified procedures for retrieval of land surface reflectance factors from satellite sensor output. Remote Sens Environ 41, 169-184.
Mountrakis, G., Im, J., Ogole, C., 2011. Support vector machines in remote sensing: a review. Photogramm Eng Remote Sens 66, 247-259.
Muller, S.V., Racoviteanu, A.E. Walker, D.A., 1999. Landsat MSS-derived land-cover map of northern Alaska: extrapolation methods and a comparison with photo-interpreted and AVHRR-derived maps. Int J Remote Sens 20, 2921–46.
Murcia, C., 1995. Edge effects in fragmented forests: implications for conservation. Trends in Ecol Evol 10(2), 58-62.
Myers, N., Mittermeier, R.A., Mittermeier, C.G., Da Fonseca, G.A., Kent, J., 2000. Biodiversity hotspots for conservation priorities. Nature 403, 853-858.
Osafo, Y.B., 2005. Reducing emissions from tropical forest deforestation: applying compensated reduction in Ghana. Tropical Deforestation and Climate Change 6372.
Owubah, C.E., Le Master, D.C., Bowker, J.M., Lee, J.G., 2001. Forest tenure systems and sustainable forest management: the case of Ghana. For Ecol Manage 149(1-3), 253-26.
Pabi, O., 2007. Understanding land-use/cover change process for land and environmental resources use management policy in Ghana. GeoJournal 68(4), 369-383.
Pal, M., 2005. Random forest classifier for remote sensing classification. Int J Remote Sens 26(1), 217-222.
Parente, L., Ferreira L., 2018. Assessing the spatial and occupation dynamics of the Brazilian pasturelands based on the automated classification of MODIS images from 2000 to 2016. Remote Sens 10(4), 606.
Park, A.B., Houghton, R.A., Hicks, G.M., Peterson, C.J., 1983. Multitemporal change detection techniques for the identification and monitoring of forest disturbances. Proceedings 17th International Symposium on Remote Sensing of Environment, Ann Arbor, MI, 77-97.
Planet Team and Planet Application Program Interface: In Space for Life on Earth. San Francisco, CA. URL https://api.planet.com (accessed on August 2018).
Potapov, P., Turubanova, S., Hansen, M.C., 2011. Regional-scale boreal forest cover and change mapping using Landsat data composites for European Russia. Remote Sens Environ 115(2), 548-561.
Pueschel, P., Buddenbaum, H., Hill, J., 2012. An efficient approach to standardizing the processing of hemispherical images for the estimation of forest structural attributes. Agric For Meteorol 160, 1–13.
Qi, J., Chehbouni, A., Huete, A.R., Kerr, Y.H., Sorooshian, S., 1994. A modified soil adjusted vegetation index. Remote Sens Environ 48, 119-126.

Ripple, W.J., Estes, J.A., Beschta, R.L., Wilmers, C.C., Ritchie, E.G., Hebblewhite, M., Berger, J., Elmhagen, B., Letnic, M., Nelson, M.P., Schmitz, O.J., Smith, D.W., Wallach, A.D., Wirsing, A.J., 2014. Status and ecological effects of the world's largest carnivores. Science 343(6167), 1241484.

Rodriguez-Galiano, V.F., Ghimire, B., Rogan, J., Chica-Olmo, M., Rigol-Sanchez, J.P., 2012. An assessment of the effectiveness of a random forest classifier for land-cover classification. Photogramm Eng Remote Sens 67, 93-104.

Ruefenacht, B., 2016. Comparison of three Landsat TM compositing methods: A case study using modeled tree canopy cover. Photogramm Eng Remote Sens 82(3), 199-211.

Schneider, A., 2012. Monitoring land cover change in urban and peri-urban areas using dense time stacks of Landsat satellite data and a data mining approach. Remote Sens Environ 124, 689-704.

Schriever, J.R., Congalton, R.G., 1995. Evaluating seasonal variability as an aid to cover-type mapping from Landsat Thematic Mapper data in the Northwest. Photogramm Eng Remote Sens 61, 321-327.

Shelestov, A., Lavreniuk, M., Kussul, N., Novikov, A., Skakun, S., 2017. Exploring Google Earth Engine platform for big data processing: classification of multi-temporal satellite imagery for crop mapping. Front Earth Sci 5, 17.

Shih, H.C., Stow, D.A., Tsai, Y.H., accepted. Guidance on and comparison of machine learning classifiers for Landsat-based land cover and land use mapping. Int J Remote Sens.

Shih, H.C., Stow, D.A., Weeks, J.R., Coulter, L.L., 2016. Determining the type and starting time of land cover and land use change in southern Ghana based on discrete analysis of dense Landsat image time series. IEEE J Sel Top Appl Earth Obs Remote Sens 9(5), 2064-2073.

Sluiter, R., Pebesma, E.J., 2010. Comparing techniques for vegetation classification using multi-and hyperspectral images and ancillary environmental data. Int J Remote Sens 31, 6143-6161.

Stow, D.A., Shih, H.C., Coulter, L.L., 2014. Discrete classification approach to land cover and land use change identification based on Landsat image time sequences. Remote Sens Lett 5(10), 922-931.

Tsai, Y.H., Stow, D.A., Chen, H.L., Lewison, R., An, L., Shi, L., 2018. Mapping vegetation and land use types in Fanjingshan National Nature Reserve using Google Earth Engine. Remote Sens 10(6), 927.

Tsai, Y.H., Stow, D.A., Shi, L., Lewison, R., An, L., 2016. Quantifying canopy fractional cover and change in Fanjingshan National Nature Reserve, China using multi-temporal Landsat imagery. Remote Sens Lett 7(7), 671-680.

Ubink, J.M., Quan, J.F., 2008. How to combine tradition and modernity? Regulating customary land management in Ghana. Land Use Policy 25(2), 198-213.

Uchida, E., Xu, J., Rozelle, S., 2005. Grain for green: cost-effectiveness and sustainability of China's conservation set-aside program. Land Econ 81, 247-264.

United Nations, 2010. The world's women 2010: Trends and statistics. United Nations, New York.

United Nations Educational, Scientific and Cultural Organization (UNESCO), 1973. International classification and mapping of vegetation. UNESCO, Paris

United Nations Environment Programme (UNEP) Global Environmet Outlook Report (GEO-5) Chapter 3: Land. UNEP, Nairobi.
Vermote, E., Justice, C., Claverie, M., Franch, B., 2016. Preliminary analysis of the performance of the Landsat 8/OLI land surface reflectance product. Remote Sens Environ 185, 46-56.
Vitousek, P.M., 1994. Beyond global warming: Ecology and global change. Ecol 75(7), 861–1876.
Wandersee, S.M., 2013. Land-cover and land-use change in human-environment systems: Understanding complex interactions among policy and management, livelihoods, and conservation. Doctoral dissertation, University of California, Santa Barbara.
Wandersee, S.M., An, L., López-Carr, D., Yang, Y., 2012. Perception and decisions in modeling coupled human and natural systems: a case study from Fanjingshan National Nature Reserve, China. Ecol. Modelling 229, 37-49.
Wang, C., Ouyang, H., Maclaren, V., Yin, Y., Shao, B., Boland, A., Tian, Y., 2007. Evaluation of the economic and environmental impact of converting cropland to forest: a case study in Dunhua county, China. J Environ Manage 85, 746-756.
Wang, C., Qi, J., Cochrane, M., 2005. Assessment of tropical forest degradation with canopy fractional cover from Landsat ETM+ and IKONOS imagery. Earth Interact 9, 1-18.
Wolter, P.T., Mladenoff, D.J., Host, G.E., Crow, T.R., 1995. Improved forest classification in the Northern Lake States using multi-temporal Landsat imagery. Photogramm Eng Remote Sens 61(9), 1129-1143.
Wu, C., 2004. Normalized spectral mixture analysis for monitoring urban composition using ETM+ imagery. Remote Sens Environ 93, 480-492.
Xie, Y., Sha, Z., Yu, M., 2008. Remote sensing imagery in vegetation mapping: a review. J Plant Ecol 1, 9-23.
Xu, J., Tao, R., Xu, Z., Bennett, M.T., 2010. China's sloping land conversion program: Does expansion equal success? Land Econ 86(2), 219-244.
Xu, J., Zhang, X., Zhang, Z., Zheng, G., Ruan, X., Zhu, J., Xi, B., 2006. Multi-scale analysis on wintering habitat selection of Reeves's pheasant (Syrmaticus reevesii) in Dongzhai national nature reserve, Henan province, China. Acta Ecol Sin 26, 2061-2067.
Yang, Y.Q., Lei, X.P., Yang, C.D., 2002. Fanjingshan Research: Ecology of the wild Guizhou snub-nosed monkey (*Rhinopithecus bieti*). Guiyang: Guizhou Science Press.
Yeh, E.T., 2009. Greening weastern China: a critical view. Geoforum 40, 884-894.
Yorke, C., Margai, F.M., 2007. Monitoring land use change in the Densu River basin, Ghana using GIS and remote sensing methods. Afr Geogr Rev 26(1), 87-110.
Yuan, F., Sawaya, K.E., Loeffelholz, B.C., Bauer, M.E., 2005. Land cover classification and change analysis of the Twin Cities (Minnesota) Metropolitan Area by multitemporal Landsat remote sensing. Remote Sens Environ 98(2-3), 317-328.
Zhou, D., Zhao, S., Zhu, C., 2012. The Grain for Green Project induced land cover change in the Loess Plateau: a case study with Ansai County, Shanxi Province, China. Ecol Indic 23, 88-94.

Zhou, H., Van Rompaey, A., 2009. Detecting the impact of the “Grain for Green” program on the mean annual vegetation cover in the Shaanxi province, China using SPOT-VGT NDVI data. Land Use Policy 26(4), 954-960.
Zhou, Z. (Ed.), 1990: Research on the Fanjing Mountain, Department of Forestry of Guizhou Province, Fanjingshan National Nature Reserve Administration Office, Guizhou, China: Guizhou People's Publishing House (in Chinese with English abstracts).